ELSEVIER

Journal of Fluids and Structures 25 (2009) 1–25

JOURNAL OF FLUIDS AND STRUCTURES

www.elsevier.com/locate/jfs

Stability of a two-dimensional airfoil with time-delayed feedback control

Y.H. Zhao*

Institute of Vibration Engineering Research, Nanjing University of Aeronautics and Astronautics, 210016 Nanjing, People's Republic of China

Received 30 June 2007; accepted 5 March 2008
Available online 9 May 2008

Abstract

This paper presents a systematic study on aeroelastic stability of a two-dimensional airfoil with a single or multiple time delays in the feedback control loops. Firstly, the delay-independent stability region of the aeroelastic system with a single time delay is determined on the basis of the generalized Sturm criterion for polynomials. Then, the stability switches with variations in time delay are analyzed when the system parameters fall out of the delay-independent stability region. Flutter boundaries of the controlled aeroelastic system as time delay varies are predicted in a continuous way by the predictor-corrector technique. Finally, two methods, the polynomial eigenvalue method and the infinitesimal generator method, are introduced to investigate the stability of the controlled aeroelastic system with multiple time delays. Numerical simulations are made to demonstrate the effectiveness of all the above approaches.

Keywords: Aeroelastic system; Time-delayed feedback control; Stability

1. Introduction

Aeroelasticity is the field of study that describes the response and stability characteristics of physical systems due to the interaction of structural, inertial and aerodynamic forces. Flutter, an important phenomenon in aeroelasticity, is the most dangerous dynamic instability that occurs when the flexible structure absorbs additional energy from the surrounding airflow. Flutter instability may decrease aircraft performance or even lead to the catastrophic failure of the structure. Furthermore, the design of the next generation of flight vehicles featuring highly flexible and highly maneuverable aircraft cruising at supersonic speed needs the active aeroelastic control technology to meet these contradictory requirements (Librescu and Marzocca, 2002). Active aeroelastic control, also called aeroservoelasticity, deals with the interaction of aerodynamics, structural dynamics, and servo control dynamics. In this field, the suppression of flutter instability by active feedback control has received particular attention (Ko et al., 1999; Platanitis and Strganac, 2004; Bhoi and Singh, 2005).

However, in most of the previous studies in aeroservoelasticity, time delays in control loops were not considered in the mathematical model of the control system. In fact, some short time delays in control loops are inevitable because of the dynamics involved in the actuators, sensors, and controllers. The time delays are prevalent when digital controllers,

*Tel.: +86 25 84891672; fax: +86 25 84892103.
E-mail address: zyhae@nuaa.edu.cn

0889-9746/$ - see front matter
doi:10.1016/j.jfluidstructs.2008.03.003

Nomenclature

a	distance from the elastic axis to midchord
$\bar{a}$	dimensionless distance of the elastic axis from midchord, $=a/b$
b	semichord of the airfoil section
c_h, c_α	damping coefficients in plunging, pitching, respectively
g_p, g_v	feedback gains in pitching displacement and pitching velocity, respectively
h	plunging displacement at the elastic axis, positive in the downward direction
I_α	mass moment of inertia of the airfoil about the elastic axis, $=mr_\alpha^2$
k_h, k_α	plunging, torsional stiffnesses, respectively
l	the number of non-zero terms in the modified sign table of the discrimination sequence
L_{qs}	quasi-steady aerodynamic lift
m	airfoil mass
r_α	radius of gyration about elastic axis
s	the number of variation of sign in the modified sign table of the discrimination sequence
s_p	span of the airfoil
t	time
T_{qs}	quasi-steady aerodynamic moment about he elastic axis of the airfoil
V, V_F	flow speed and flutter speed of the uncontrolled system
x_α	the distance of the elastic axis from center of mass
α	pitching angle, positive in the nose-up rotation
λ, λ_c	eigenvalues of the controlled and uncontrolled system, respectively
ρ_a	air density
τ, τ_1, τ_2	time delays
τ_c, τ_{cm}, τ_{ck}	critical time delays
ω_F	flutter frequency of the uncontrolled system
$\Omega, \bar{\Omega}$	parameter spaces

analogue anti-aliasing and reconstruction filters, and hydraulic actuators are used (Hu et al., 1998). These time delays become particularly significant when the control effort demands large control forces or high frequencies. It is therefore crucial to understand the effect of time delays on control systems. On the one hand, applications of unsynchronized control forces due to time delay may result in a degradation of the control performance and may even render the controlled structures unstable, but on the other hand, an appropriate time delay may stabilize an unstable system (Wang and Hu, 2000).

From theoretical aspects of time delay systems, it is well known that a controlled system is asymptotically stable if all the roots of the corresponding characteristic equation have negative real parts. For a linear time-invariant system with time delays, however, the characteristic equation becomes transcendental due to the exponential functions associated with time delays. The transcendentality brings an infinite number of characteristic roots, which are cumbersome to handle, as evident from the literature (Niculescu, 2001). To resolve this difficulty, a number of methodologies have been suggested that assess the stability of time delay systems, such as Stépán–Hassard method (Stépán, 1989; Hassard, 1997), D-subdivision method (Kolmanovski and Nosov, 1986), and its modified version (Olgac and Sipahi, 2002). In Wang and Hu (2000), the generalized Sturm criterion was used to determine whether a polynomial equation has positive real roots. In Hu et al. (1998) the stability of the high dimensional system involving feedback delay was investigated through the perturbation approach to trace the evolution of the eigenvalues. Time delays also give rise to more difficulties in the analysis of the nonlinear control system. For example, it has been shown that the nonlinear oscillators with a single time delay may undergo Hopf bifurcation or more complicated bifurcations such as Hopf–Hopf bifurcation, and chaotic behaviors. In Hu and Wang (2002), systematic approaches to the problem of stability for the nonlinear system with time delays have been addressed in detail.

In the field of aeroservoelasticity, the stability and stabilization of the aeroelastic system with time-delayed feedback control have received much attention in recent years. In Ramesh and Narayanan (2001), for example, the chaotic motions of a two-dimensional airfoil with cubic pitching stiffness and linear viscous damping were controlled by using the time-delayed feedback in the form of Pyragas. Four control strategies were implemented with plunging displacement, plunging velocity, pitching angle and pitching velocity as the feedback signals. The study showed that the system could be stabilized to a periodic motion if the control was generated by either measuring the plunging displacement, or pitching angle, or pitching velocity. The results demonstrated that the feedback control signal derived from the measurement of the pitching variables is more effective in controlling the chaotic motion of the airfoil. Yuan et al. (2004) investigated the effect of the time-delayed feedback control on the flutter instability boundary of a two-dimensional supersonic lifting surface. They demonstrated that the time delay in the nonlinear feedback control could have a profound effect on the stability of the bifurcation motions. For example, it could transform a subcritical Hopf

bifurcation to a supercirtical one. In Marzocca and Librescu (2005) the effects of time delay on the feedback control of two-dimensional lifting surfaces in an incompressible flow-field was investigated. The stability behavior of aeroelastic systems with nonlinear time-delayed feedback was analyzed via Pontryagin's approach in conjunction with Stepan's theorems and the associated aeroelastic Volterra kernels. It was found that with proper design, the time delay could be a more efficient way to control instability than the conventional control strategies without time delay. In Librescu and Marzocca (2005), the flutter instability of actively controlled airfoils involving a time-delayed feedback control was investigated via Stepan's theorems. It was observed that any value of time delay could be detrimental from the point of view of the aeroelastic response, but short time delays might be beneficial from the point of view of flutter instability.

The primary aim of this paper is to gain a comprehensive insight into the stability problem of the controlled aeroelastic system with time-delayed feedback. We concentrate on the delay-independent stability, stability switches of the aeroelastic system with a single time delay, and efficient numerical methods for the multiple time delays case. The results given in this paper can be used as the basic material to design more advanced control systems with time delays. The paper is organized as follows. In Section 2, the aeroelastic equation of an airfoil with a single time delay in feedback loop is established. In Section 3, the generalized Sturm criterion and the predictor-corrector method are used to predict the stability of the controlled aeroelastic system with a single time delay. Section 4 presents an approach to compute critical time delays of the system with multiple time delays. In Section 5, the rightmost eigenvalues of the linear aeroelastic system with multiple time delays are determined by solving the eigenvalue problem for an approximation matrix to the infinitesimal generator. In Section 6, several conclusions are drawn.

2. Aeroelastic equations of the controlled system

The study begins with an airfoil oscillating in pitch and plunge, as shown in Fig. 1, where the plunging deflection is denoted by h, positive downward direction, and the pitching angle is α, positive nose up. Furthermore, b is the semi-chord length, x_a the distance of the elastic axis from center of mass, $\bar{a}$ the dimensionless distance of the elastic axis from midchord, k_h the plunging stiffness, k_α the torsional stiffness, and V the flow speed.

For the traditional models in aeroelastic control, no time delay is taken into consideration. However, because of the delay phenomena, the feedback is done with the outdated state of the system. For convenience, we assume that the control strategy is implemented with the pitching velocity as the time-delayed feedback signal, thus the closed-loop aeroelastic equations of the airfoil can be expressed as

$$m\ddot{h} + mx_\alpha\ddot{\alpha} + c_h\dot{h} + k_h h = -L_{qs}(t), \tag{1}$$

$$mx_\alpha\ddot{h} + mr_\alpha^2\ddot{\alpha} + c_\alpha\dot{\alpha} + k_\alpha\alpha = T_{qs}(t) + g_v\dot{\alpha}(t-\tau), \tag{2}$$

where g_v is the velocity feedback gain, and $\tau \geqslant 0$ is the time delay in the feedback. The definitions of other parameters can be found in Nomenclature.

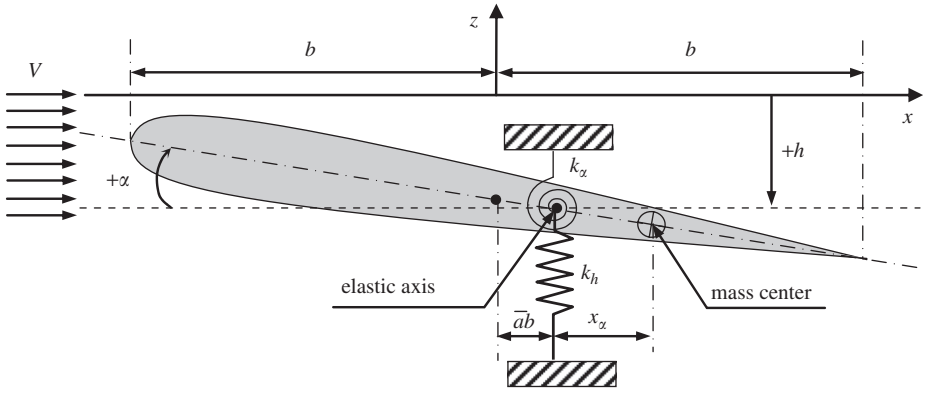

Fig. 1. Schematic figure of a 2-dof airfoil.

For a two-dimensional and incompressible flow, the quasi-steady aerodynamic lift and moment are given by (Zhao, 2007)

$$L_{qs} = \pi\rho_a b^2 s_p(\ddot{h} + V\dot{\alpha} - b\bar{a}\ddot{\alpha}) + 2\pi\rho_a V b s_p\left[V\alpha + \dot{h} + b\left(\tfrac{1}{2} - \bar{a}\right)\dot{\alpha}\right], \tag{3}$$

$$T_{qs} = \pi\rho_a b^2 s_p\left[b\bar{a}\ddot{h} - Vb\left(\tfrac{1}{2} - \bar{a}\right)\dot{\alpha} - b^2\left(\tfrac{1}{8} + \bar{a}^2\right)\ddot{\alpha}\right] + 2\pi\rho_a V b^2 s_p\left(\bar{a} + \tfrac{1}{2}\right)\left[V\alpha + \dot{h} + b\left(\tfrac{1}{2} - \bar{a}\right)\dot{\alpha}\right]. \tag{4}$$

Combining Eqs. (1)–(4), we have the following aeroelastic equations:

$$c_0\ddot{h}(t) + c_1\ddot{\alpha}(t) + c_2\dot{h}(t) + c_3\dot{\alpha}(t) + c_4 h(t) + c_5\alpha(t) = 0, \tag{5}$$

$$d_0\ddot{h}(t) + d_1\ddot{\alpha}(t) + d_2\dot{h}(t) + d_3\dot{\alpha}(t) + d_4 h(t) + d_5\alpha(t) = g_v\dot{\alpha}(t-\tau), \tag{6}$$

where $c_0, \ldots, c_5$ and $d_0, \ldots, d_5$ are given in Appendix A.

The closed-loop aeroelastic equation in the compact state space form can be written as

$$\dot{\boldsymbol{X}} = \boldsymbol{A}_0(V)\boldsymbol{X} + \boldsymbol{A}_2(g_v)\boldsymbol{X}(t-\tau), \tag{7}$$

where $\boldsymbol{X} = [h \quad \alpha \quad \dot{h} \quad \dot{\alpha}]^{\mathrm{T}}$, the matrices $\boldsymbol{A}_0$ and $\boldsymbol{A}_2$ are given in Appendix B.

3. Stability analysis of the controlled system with a single time-delay

3.1. Delay-independent stability

A system is said to be delay-independently stable if it is asymptotically stable for arbitrary time delays, that is, the system stability is independent of time delays. To find the parametric region of the delay-independent stability of Eq. (7), we substitute the candidate solution $\boldsymbol{X} = \bar{\boldsymbol{X}}\,\mathrm{e}^{\lambda t}$ into Eq. (7), which yields the following characteristic equation:

$$\det(\lambda\boldsymbol{I} - \boldsymbol{A}_0(V) - \boldsymbol{A}_2(g_v)\,\mathrm{e}^{-\lambda\tau}) = 0. \tag{8}$$

The above characteristic equation can be expanded as follows:

$$D(\lambda,\tau) = P(\lambda) + Q(\lambda)\,\mathrm{e}^{-\lambda\tau} = 0, \tag{9}$$

where $P(\lambda)$ and $Q(\lambda)$ are two polynomials of real coefficients, and are given in Appendix C. The conditions for the delay-independent stability of Eq. (7) can be stated as follows (Hu and Wang, 2002).

Theorem 1. *The linear system governed by Eq.* (7) *is delay-independently stable if and only if the following two conditions hold true:*

(a) *the characteristic polynomials* $P(\lambda) + Q(\lambda)$, *corresponding to the case* $\tau = 0$, *is Hurwitz stable*;
(b) *the marginal stability condition* $D(\mathrm{i}\omega,\tau) = 0$ *has no real root* ω *for all given time delay* $\tau \geqslant 0$.

For the first condition, the Routh–Hurwitz stability conditions that govern the asymptotic stability of the system are given by

$$\begin{cases} R_1 = p_3 + q_3 > 0, \\ R_2 = p_2 + q_2 > 0, \\ R_3 = p_0 > 0, \\ R_4 = (p_1 + q_1)[(p_3 + q_3)(p_2 + q_2) - (p_1 + q_1)] - (p_3 + q_3)^2 p_0 > 0. \end{cases} \tag{10}$$

For the second condition, the generalized Strum criterion can be used to determine whether $D(\mathrm{i}\omega,\tau) = 0$ has any real roots or not. For this purpose, let

$$\begin{cases} P_R(\omega) = \mathrm{Re}[P(\mathrm{i}\omega)], \quad P_I(\omega) = \mathrm{Im}[P(\mathrm{i}\omega)], \\ Q_R(\omega) = \mathrm{Re}[Q(\mathrm{i}\omega)], \quad Q_I(\omega) = \mathrm{Im}[Q(\mathrm{i}\omega)]. \end{cases} \tag{11}$$

From $D(\mathrm{i}\omega,\tau)=0$, we can then separate the polynomial into its real and imaginary parts, and write the exponential in terms of trigonometric functions to get

$$P_R(\omega)+\mathrm{i}P_I(\omega)+(Q_R(\omega)+\mathrm{i}Q_I(\omega))\times(\cos(\omega\tau)-\mathrm{i}\,\sin(\omega\tau))=0. \tag{12}$$

Because $\mathrm{i}\omega$ is purely imaginary, P_R and Q_R are even polynomials of ω, whereas P_I and Q_I are odd polynomials. In order that Eq. (12) holds, both the real and imaginary parts must be zero. That is,

$$P_R(\omega)+Q_R(\omega)\cos(\omega\tau)+Q_I(\omega)\sin(\omega\tau)=0, \tag{13}$$

$$P_I(\omega)-Q_R(\omega)\sin(\omega\tau)+Q_I(\omega)\cos(\omega\tau)=0. \tag{14}$$

In order that Eq. (9) has a pair of pure imaginary roots $\pm\mathrm{i}\omega$ for $\tau\geqslant 0$, it is necessary that $|P(\mathrm{i}\omega)|^2=|Q(\mathrm{i}\omega)|^2$ holds, that is

$$F(\omega)=P_R^2(\omega)+P_I^2(\omega)-(Q_R^2(\omega)+Q_I^2(\omega))=0, \tag{15}$$

has a positive root ω. Note that this is a polynomial equation without any trigonometric terms involving delay τ, the quasi-polynomial $D(\mathrm{i}\omega,\tau)=0$ has no real roots ω for $\tau\geqslant 0$, if and only if

$$F(\omega)=0 \tag{16}$$

has no real roots (except for zero).

For the aeroelastic system described by Eq. (7), $F(\omega)$ can be expressed as

$$F(\omega)=\omega^8+b_1\omega^6+b_2\omega^4+b_3\omega^2+b_4, \tag{17}$$

where

$$b_1=-2p_2+p_3^2-q_3^2,\quad b_2=2p_0+p_2^2-2p_1p_3+2q_1q_3-q_2^2,\quad b_3=p_1^2-2p_0p_2-q_1^2,\quad b_4=p_0^2.$$

In the generalized Sturm criterion, the discrimination sequence plays a central role in determining the number of real roots of polynomial $F(\omega)$. The MAPLE routine *discr* (Hu and Wang, 2002) enables one to derive the discrimination sequence $D_1(F)-D_8(F)$ as follows

$$1,\ d_0,\ d_0d_1,\ d_1d_2,\ d_2d_3,\ d_3d_4,\ d_4d_5,\ d_5^2d_6 \tag{18}$$

where d_0-d_6 are given in Appendix D.

Parameters used for numerical simulations are presented in Table 1. Obviously, the Routh–Hurwitz conditions $R_2>0$ and $R_3>0$ hold true in the parameter space shown in Fig. 2. If the parameter combination (g_v, V) falls into the hatched region in Fig. 2 for $\tau=0.0\,\mathrm{s}$, then the system is Routh–Hurwitz stable. The point of intersection of the two curves $R_4=0$ and $g_v=0$ represents the flutter point of the uncontrolled system, which reveals that the flutter speed of the system is $V_F=23.45\,\mathrm{m/s}$. An alternative method to obtain the flutter speed of the uncontrolled system is to compute the eigenvalue λ_c of the system matrix $\boldsymbol{A}_0(V)$ under various flow speeds, as shown in Fig. 3. To validate the stability of this delay-free system, the plunging and pitching time histories of the airfoil for three different flight speeds, $V=23, 23.45, 23.55\,\mathrm{m/s}$, are computed, as shown in Fig. 4. It can be seen from Fig. 4 that the responses of the airfoil are asymptotically stable for $V<V_F$, unstable for $V>V_F$, and maintain sustained oscillation for $V=V_F$.

Table 1
The system parameters for simulations

$s_p=1.0\,\mathrm{m}$
$m=2.049\,\mathrm{kg}$
$k_\alpha=6.833\,\mathrm{N\,m/rad}$
$I_\alpha=mx_\alpha^2+0.0517\,\mathrm{kg\,m^2}$
$b=0.135\,\mathrm{m}$
$k_h=2844.4\,\mathrm{N/m}$
$x_\alpha=[0.0873-(1+\bar{a})b]\,\mathrm{m}$
$c_\alpha=0.036\,\mathrm{N\,s/rad}$
$\rho_a=1.225\,\mathrm{kg/m^3}$
$\bar{a}=-0.6847$
$c_h=27.43\,\mathrm{N\,s/m}$
$V_F=23.45\,\mathrm{m/s}$

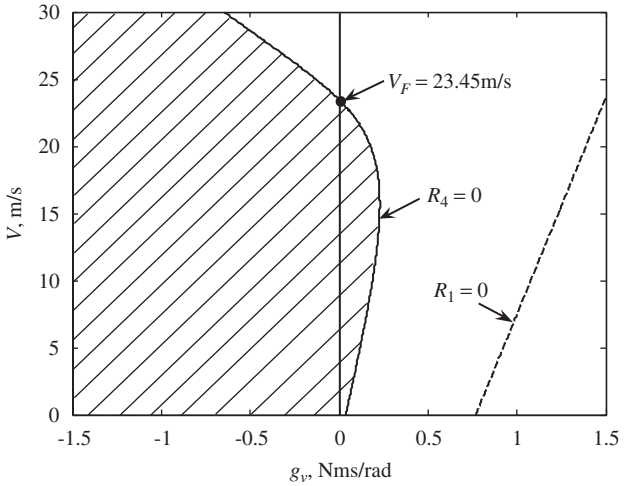

Fig. 2. Routh–Hurwitz stable region, $\tau = 0.0$ s.

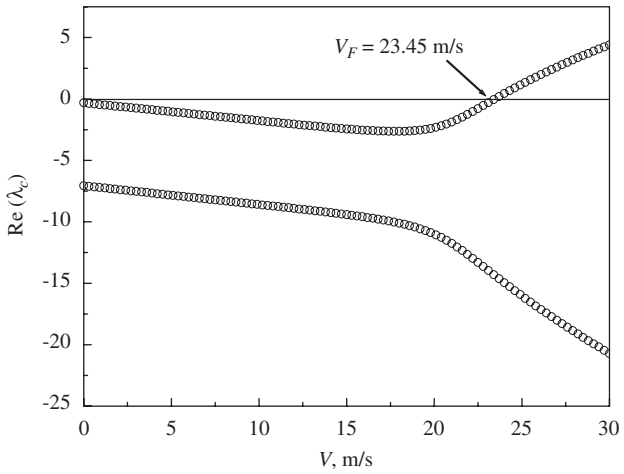

Fig. 3. Root loci of open loop system, $\tau = 0.0$ s.

To obtain the parametric region of the delay-independent stability of the system, we consider the following parameter space:

$$\Omega = \{(g_v, V) | |g_v| \leqslant 1.5, 0 \leqslant V \leqslant 30\}. \tag{19}$$

We can easily verify that $d_0 > 0$, $d_2 < 0$, $d_3 < 0$, $d_4 < 0$, and $d_6 > 0$ always hold. As shown in Fig. 5, the stable region in the Routh–Hurwitz sense is divided by curves $d_1 = 0$, $d_5 = 0$ and $R_4 = 0$ into four sub-regions marked by I, II, III, and IV respectively. The modified sign tables of the corresponding discrimination sequence in each sub-region are listed in Table 2. If the parameter combination (g_v, V) falls into regions II and IV in Fig. 5, then we have $d_0 > 0$, $d_1 < 0$, $d_2 < 0$, $d_3 < 0$, $d_4 < 0$, $d_5 > 0$, and $d_6 > 0$. Hence the modified sign table is [1 1 −1 1 1 1 −1 1 0], the number of variation of signs is 4, and $l - 2s = 0$ holds. Based upon the generalized Sturm criterion, we conclude that $F(\omega) = 0$ has no real roots; thus, according to Theorem 1, the system is delay-independently stable in sub-regions II and IV. In sub-region I, we have $d_0 > 0$, $d_1 < 0$, $d_2 < 0$, $d_3 < 0$, $d_4 < 0$, $d_5 < 0$, and $d_6 > 0$, the modified sign table is [1 1 −1 1 1 1 1 1 1], and the number of variation of signs is 2. Thus, $F(\omega) = 0$ has $l/2s = 2$ distinct real roots. In the same way, we can see that $F(\omega) = 0$ has two distinct real roots in sub-region III.

In what follows we attempt to verify the region obtained of the delay-independent stability of the system by solving the delay differential Eq. (7) in the time domain. For this purpose, within the delay-independent stability region, we

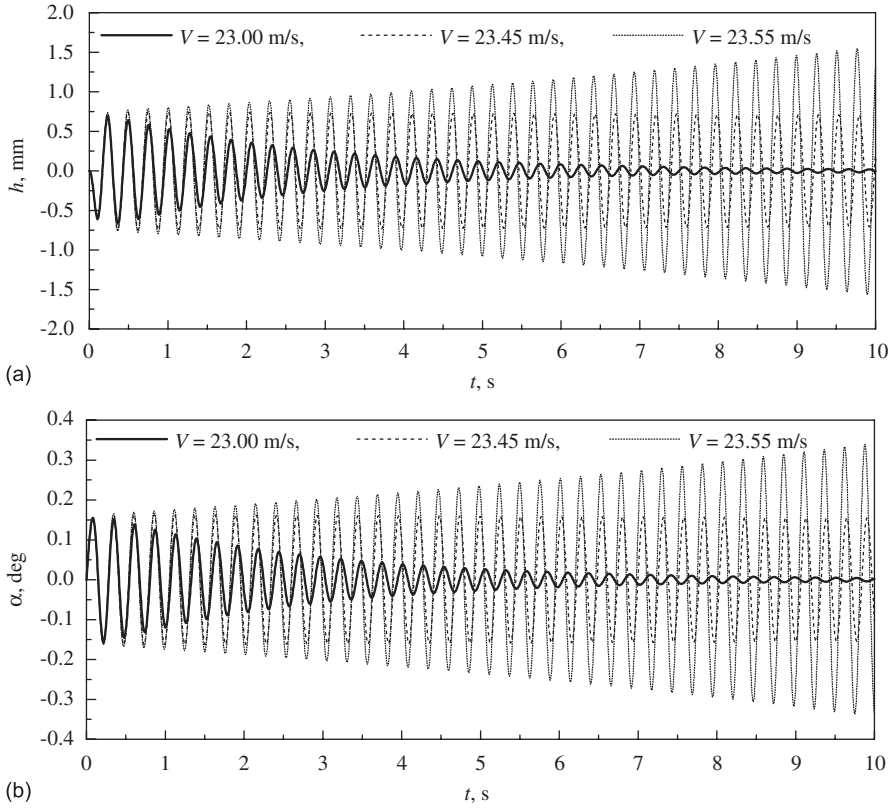

Fig. 4. Time history of the system, $\tau = 0.0$ s: (a) plunging response and (b) pitching response.

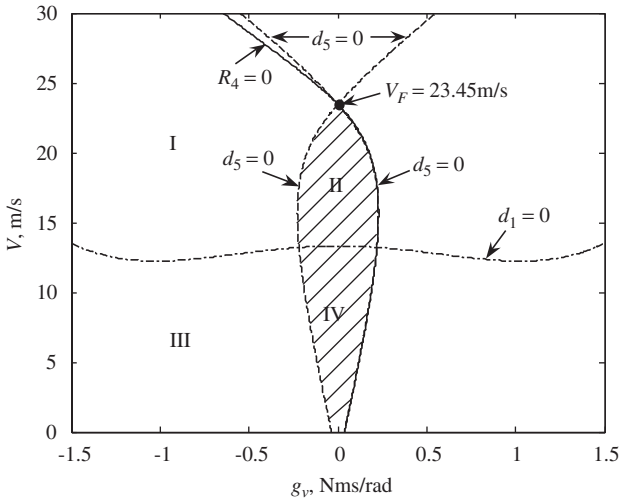

Fig. 5. Delay-independent stable region of the system.

take the velocity feedback gain g_v as 0.15 N m s/rad, and the flow speed V as 20 m/s. The plunging and pitching responses of the system for different time delays ($\tau = 10$ and 30 ms) are shown in Fig. 6. Obviously, the system is asymptotically stable for those time delays. In fact, an arbitrary time delay can be used in the numerical simulations to verify the delay-independent stability.

Table 2
The sign tables of the discrimination sequence of $F(\omega)$ (used for analyzing delay-independent stability)

Sub-region	S_1	S_2	S_3	S_4	S_5	S_6	S_7	S_8	$l-2s$
I	1	1	−1	1	1	1	1	1	4
II	1	1	−1	1	1	1	−1	1	0
III	1	1	1	−1	1	1	1	1	4
IV	1	1	1	−1	1	1	−1	1	0

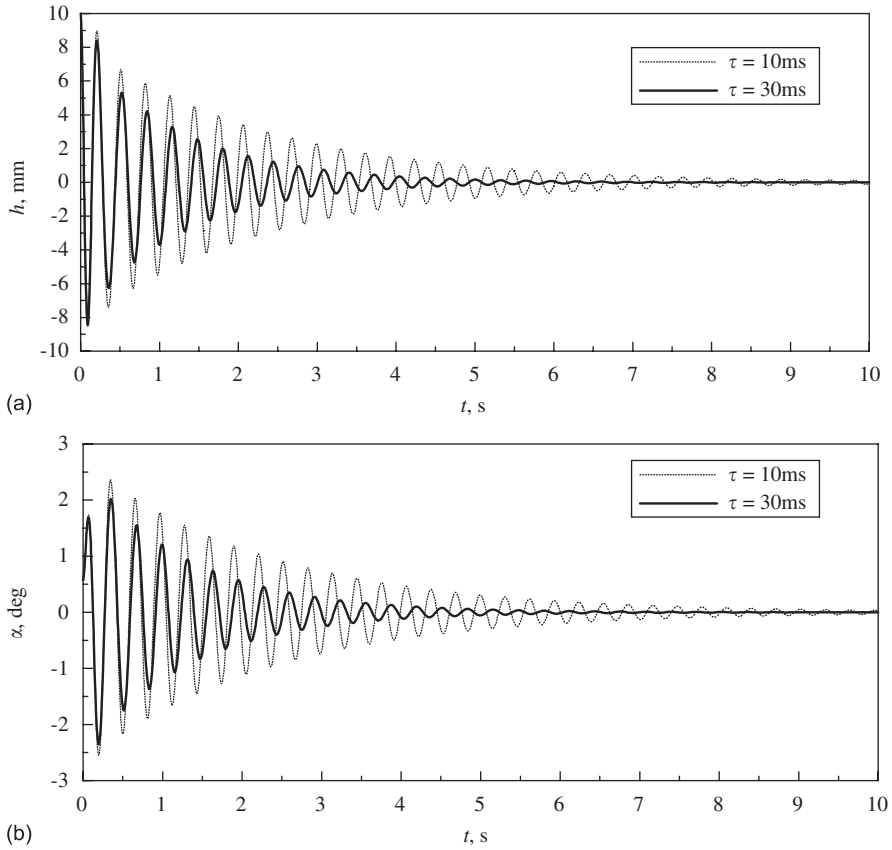

Fig. 6. Responses when system parameters fall into delay-independent stable region: (a) plunging response and (b) pitching response.

In summary, within the parameter space Ω, the system is delay-independently stable if and only if the parameter combination falls into sub-regions II and IV in Fig. 5. No region of the delay-independent stability of the system exists when the flow speed $V > V_F$. This is an important feature of the controlled aeroelastic system.

3.2. Stability switches

For the aeroelastic system, the delay-independently stable region only exists in the range of the flow speed which is less than the flutter speed of the open loop system. In practical applications, the delay-independently stable region is usually a very small part in the parameter space. If the system parameters do not fall into the delay-independent stable region, the real part of at least one characteristic root changes its sign when the time delay varies. That is, the stability of the controlled system cannot keep unchanged with an increase of time delay. Such a change with increase of time delay is referred to as the stability switch.

Note that, once a positive root ω of $F(\omega)$ is found, the critical time delays are given by

$$\tau_{ck} = \frac{\theta}{\omega} + \frac{2k\pi}{\omega}, \quad k = 0, 1, 2, \ldots. \tag{20}$$

where $\theta \in [0, 2\pi)$ satisfies a set of triangle equations

$$\begin{cases} \sin\theta = \dfrac{P_I(\omega)Q_R(\omega) - P_R(\omega)Q_I(\omega)}{Q_R^2(\omega) + Q_I^2(\omega)}, \\ \cos\theta = -\dfrac{P_R(\omega)Q_R(\omega) + P_I(\omega)Q_I(\omega)}{Q_R^2(\omega) + Q_I^2(\omega)}. \end{cases} \tag{21}$$

As analyzed in Wang and Hu (2000), if $F(\omega) = 0$ has no real root, the system does not undergo any stability switches as the time delay τ increases. That is, the system is delay-independently stable if it is asymptotically stable when the time delay disappears, or unstable for an arbitrary time delay if the delay-free system is unstable. If $F(\omega) = 0$ has any real roots, the root λ of Eq. (9) can be regarded as a function of τ. Once a pair of pure imaginary characteristic roots $\pm i\omega$ is found, the corresponding critical values of time delay in Eq. (20) can be determined. Here we assume that $\pm i\omega$ are not a pair of repeated characteristic roots. To assess the tendency of imaginary roots, we have the following equation

$$S = \operatorname{sgn}\left\{ \operatorname{Re}\left[\frac{d\lambda(\tau)}{d\tau}\right]\Bigg|_{\lambda=i\omega} \right\} = \operatorname{sgn}(F'(\omega)). \tag{22}$$

The generalized Sturm criterion can be used to analyze the stability switch of the controlled system with time delay, thus we have the following theorem (Hu and Wang, 2002).

Theorem 2. *Assume that Eq.* (9) *has no pure imaginary characteristic roots satisfying* $Q(i\omega) = 0$ *and the roots of* $F(\omega)$ *are simple. Let* l *and* s *be the number of non-zero terms and the number of variation of sign in the modified sign table of the discrimination sequence of* $F(\omega)$*, then following facts are true*:

(a) *If* $l - 2s = 0$, *the system is delay-independent stable or unstable for any time delay, depending on whether the system free of time delay is asymptotically stable or not.*
(b) *If* $l - 2s = 2$ *and the system free of time delay is asymptotically stable, there exists a critical time delay* $\tau_c > 0$ *such that the system remains asymptotically stable when* $\tau \in [0, \tau_c)$, *and becomes unstable when* $\tau \geqslant \tau_c$. *If* $l - 2s = 2$ *and the system is unstable for* $\tau = 0$, *it keeps unstable for an arbitrary time delay* τ.
(c) *If* $l - 2s > 2$, *a finite number of stability switches occurs as time delay* τ *increases and the system becomes unstable at last.*

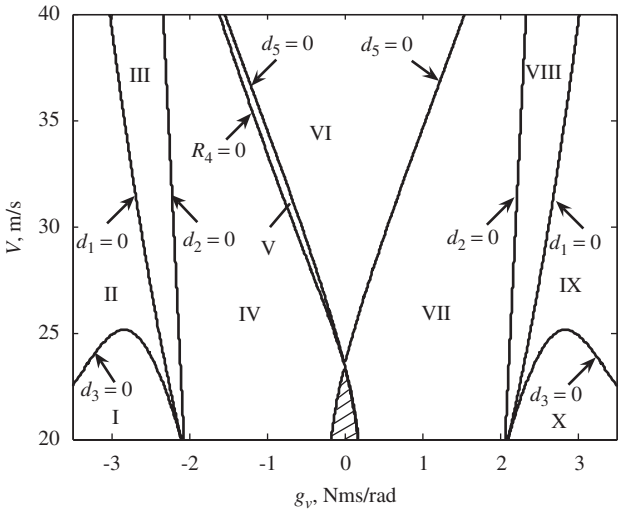

Fig. 7. Regions divided by curves.

Table 3
The sign tables of the discrimination sequence of $F(\omega)$ (used for analyzing stability switches)

Sub-region	D_0	d_1	d_2	d_3	d_4	d_5	d_6	S_1	S_2	S_3	S_4	S_5	S_6	S_7	S_8	$l-2s$
I, X	+	+	+	+	−	−	+	1	1	1	1	1	−1	1	1	4
II, IX	+	+	+	−	−	−	+	1	1	1	1	−1	1	1	1	4
III, VIII	+	−	+	−	−	−	+	1	1	−1	−1	−1	1	1	1	4
IV, VII	+	−	−	−	−	−	+	1	1	−1	1	1	1	1	1	4
V	+	−	−	−	−	−	+	1	1	−1	1	1	1	1	1	4
VI	+	−	−	−	−	+	+	1	1	−1	1	1	1	−1	1	0

To apply this theorem to aeroelastic simulations, we consider the parameter region defined by

$$\bar{\Omega} = \{(g_v, V) || g_v | \leqslant 3.5\,\mathrm{N\,m\,s/rad}, 20\,\mathrm{m/s} \leqslant V \leqslant 40\,\mathrm{m/s}\}. \tag{23}$$

Fig. 7 shows that the curves $d_1 = 0$, $d_2 = 0$, $d_3 = 0$, $d_5 = 0$, and $R_4 = 0$ divide the region $\bar{\Omega}$ into 10 sub-regions (except for delay-independent stable region), which are numbered by I, II,…,X. The sign tables of the discrimination sequence of the system are shown in Table 3. As can be seen, $F(\omega)$ has no real roots and the system is unstable for $\tau = 0$, so the aeroelastic system is unstable for arbitrary time delay $\tau \geqslant 0$ when the parameter combination (g_v, V) falls into the sub-region VI. $F(\omega)$ always has two positive real roots when the parameter combination (g_v, V) falls into other sub-regions except for sub-region VI. In the following, the stability switches of the system will be demonstrated through a few case studies.

Case 1. $g_v = -1.0\,\mathrm{N\,m\,s/rad},\ V = 25.0\,\mathrm{m/s}$

This parameter combination (g_v, V) falls into the sub-region IV in Fig. 7. It is easy to know that the polynomial $F(\omega)$ has two distinct real roots $\omega_1 = 33.8544$ and $\omega_2 = 15.3061$ satisfying $F'(\omega_1) > 0$ and $F'(\omega_2) < 0$, respectively. The corresponding critical values of time delay are

$$\begin{cases} \tau_{c1,0} = 0.0293, & \tau_{c1,1} = 0.2149, & \tau_{c1,2} = 0.4005, & \tau_{c1,3} = 0.5861, & \tau_{c1,4} = 0.7717, \\ \tau_{c2,0} = 0.2957, & \tau_{c2,1} = 0.7062, & \tau_{c2,2} = 1.1167, & \tau_{c2,3} = 1.5272, & \tau_{c2,4} = 1.9377. \end{cases} \tag{24}$$

They can be ranked as

$$\underline{\tau_{c1,0} < \tau_{c1,1}} < \tau_{c2,0} < \tau_{c1,2} < \tau_{c1,3} < \tau_{c2,1} < \cdots. \tag{25}$$

Because the system is asymptotically stable for $\tau = 0$ and $F'(\omega_1) > 0$, the controlled system is asymptotically stable for $\tau \in [0, \tau_{c1,0})$. As the time delay τ increases, a pair of conjugate roots cross the pure imaginary axis, so the characteristic equation of system adds a new pair conjugate roots with positive real parts for crossing at $\tau_{c1,0}$. Increasing the time delay further, the characteristic equation of the system has a root with positive real part, so the system is unstable for $\tau \in (\tau_{c1,0}, \tau_{c1,1})$. As a result, with the increase of time delay, the characteristic equation of system adds another new pair of conjugate roots with positive real parts for crossing at $\tau_{c1,1}$, so the controlled system is unstable when $\tau \in (\tau_{c1,1}, \tau_{c2,0})$. Note that the following inequalities hold:

$$\tau_{c1,k+1} - \tau_{c1,k} = \frac{2\pi}{\omega_1} < \frac{2\pi}{\omega_2} = \tau_{c2,k+1} - \tau_{c2,k}, \quad \tau_{c1,0} < \tau_{c2,0}. \tag{26}$$

Based on the above inequalities, we conclude that in Eq. (25) $\tau_{c1,0}$ is followed immediately by $\tau_{c1,1}$, but any $\tau_{c2,k}$ cannot be flowed by $\tau_{c2,k+1}$. Therefore, the system has at least one pair of characteristic roots with positive real part if $\tau > \tau_{c1,0}$. This implies that the equilibrium of system is unstable as long as $\tau > \tau_{c1,0}$ holds.

Therefore, the system undergoes a stability switch once as the time delay varies from zero to infinity. Fig. 8 shows the detrimental effect of the delay on the aeroelastic response. It can be seen that time delay causes responses of the system to attenuate for $\tau = 0.028\,\mathrm{s} \in [0, \tau_{c1,0})$, and to diverge for $\tau = 0.030\,\mathrm{s} \in (\tau_{c1,0}, \tau_{c1,1})$.

Case 2. $g_v = -2.3\,\mathrm{N\,m\,s/rad},\ V = 25.0\,\mathrm{m/s}$

This parameter combination (g_v, V) falls into the sub-region, in Fig. 7, and the polynomial $F(\omega)$ has two distinct real roots $\omega_1 = 46.3558$ and $\omega_2 = 8.8656$ satisfying $F'(\omega_1) > 0$ and $F'(\omega_2) < 0$, respectively. The corresponding critical values

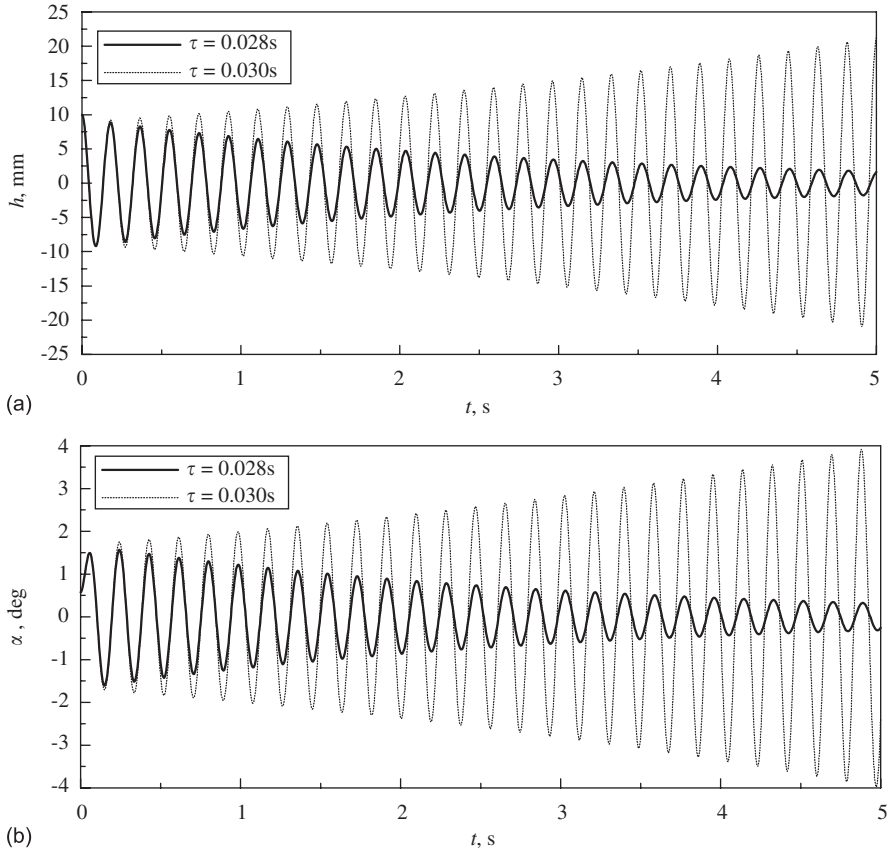

Fig. 8. Responses of the controlled aeroelastic system with time delay: (a) plunging response and (b) pitching response.

of time delay are

$$\begin{cases} \tau_{c1,0} = 0.0305, & \tau_{c1,1} = 0.1661, & \tau_{c1,2} = 0.3016, & \tau_{c1,3} = 0.4372, & \tau_{c1,4} = 0.5727, \\ \tau_{c2,0} = 0.5193, & \tau_{c2,1} = 1.2281, & \tau_{c2,2} = 1.9368, & \tau_{c2,3} = 2.6455, & \tau_{c2,4} = 3.3542. \end{cases} \tag{27}$$

They are ranked as

$$\underline{\tau_{c1,0} < \tau_{c1,1} < \tau_{c1,2} < \tau_{c1,3}} < \tau_{c2,0} < \tau_{c1,4} < \cdots \tag{28}$$

One can similarly find that the system is asymptotically stable for $\tau \in [0, \tau_{c1,0})$, and unstable for $\tau > \tau_{c1,0}$. The system undergoes the stability switch once as time delay varies from zero to infinity.

Case 3. $g_v = -3.0\,\mathrm{N\,m\,s/rad},\ V = 30.0\,\mathrm{m/s}$

This parameter combination (g_v, V) falls into the sub-region II in Fig. 7, and the polynomial $F(\omega)$ has two distinct positive real roots $\omega_1 = 56.2742$ and $\omega_2 = 9.2920$ satisfying $F'(\omega_1) > 0$ and $F'(\omega_2) < 0$, respectively. The corresponding critical values of time delay are

$$\begin{cases} \tau_{c1,0} = 0.0265, & \tau_{c1,1} = 0.1381, & \tau_{c1,2} = 0.2498, & \tau_{c1,3} = 0.3614, & \tau_{c1,4} = 0.4731, & \tau_{c1,5} = 0.5848, \\ \tau_{c2,0} = 0.5002, & \tau_{c2,1} = 1.1764, & \tau_{c2,2} = 1.8526, & \tau_{c2,3} = 2.5288, & \tau_{c2,4} = 3.2050, & \tau_{c2,5} = 3.8812. \end{cases} \tag{29}$$

They are sorted as

$$\underline{\tau_{c1,0} < \tau_{c1,1} < \tau_{c1,2} < \tau_{c1,3} < \tau_{c1,4}} < \tau_{c2,0} < \tau_{c1,5} < \cdots. \tag{30}$$

We claim that the system is asymptotically stable for $\tau \in [0, \tau_{c1,0})$, and unstable for $\tau > \tau_{c1,0}$.

Case 4. $g_v = -3.0\,\mathrm{N\,m\,s/rad},\ V = 24.0\,\mathrm{m/s}$

This parameter combination (g_v, V) falls into the sub-region I in Fig. 7, and the polynomial $F(\omega)$ has two distinct positive real roots $\omega_1 = 58.2388$ and $\omega_2 = 6.7238$ satisfying $F'(\omega_1)>0$ and $F'(\omega_2)<0$, respectively. The corresponding critical values of time delay are

$$\begin{cases} \tau_{c1,0} = 0.0267, & \tau_{c1,1} = 0.1346, & \tau_{c1,2} = 0.2425, & \tau_{c1,3} = 0.3504, & \tau_{c1,4} = 0.4582, & \tau_{c1,5} = 0.5661, \\ \tau_{c1,6} = 0.6740, & \tau_{c1,7} = 0.7819, & & & & \\ \tau_{c2,0} = 0.6878, & \tau_{c2,1} = 1.6223, & \tau_{c2,2} = 2.5568, \tau_{c2,3} = 3.4912, & \tau_{c2,4} = 4.4257, & \tau_{c2,5} = 5.3602, & \\ \tau_{c2,6} = 6.2947, & \tau_{c2,7} = 7.2291. & & & & \end{cases} \tag{31}$$

We rank these critical time delays as

$$\underline{\tau_{c1,0} < \tau_{c1,1} < \tau_{c1,2} < \tau_{c1,3} < \tau_{c1,4} < \tau_{c1,5} < \tau_{c1,6}} < \tau_{c2,0} < \cdots. \tag{32}$$

Obviously, the system is asymptotically stable for $\tau \in [0, \tau_{c1,0})$, and unstable for $\tau > \tau_{c1,0}$.

Case 5. $g_v = 1.0\,\mathrm{N\,m\,s/rad},\ V = 25.0\,\mathrm{m/s}$

This parameter combination (g_v, V) falls into the sub-region VII in Fig. 7, and the polynomial $F(\omega)$ has two distinct positive real roots $\omega_1 = 33.8544$ and $\omega_2 = 15.3061$ satisfying $F'(\omega_1)>0$ and $F'(\omega_2)<0$, respectively. The corresponding critical values of time delay are

$$\begin{cases} \tau_{c1,0} = 0.1221, & \tau_{c1,1} = 0.3077, & \tau_{c1,2} = 0.4933, & \tau_{c1,3} = 0.6789, & \tau_{c1,4} = 0.8645, & \tau_{c1,5} = 1.0501, \\ \tau_{c2,0} = 0.0904, & \tau_{c2,1} = 0.5009, & \tau_{c2,2} = 0.9115, & \tau_{c2,3} = 1.3220, & \tau_{c2,4} = 1.7325, & \tau_{c2,5} = 2.1430. \end{cases} \tag{33}$$

We sort these critical time delays as

$$\tau_{c2,0} < \underline{\tau_{c1,0} < \tau_{c1,1} < \tau_{c1,2}} < \tau_{c2,1} < \tau_{c1,3} < \cdots. \tag{34}$$

Clearly, the controlled system is unstable for $\tau \in [0, \tau_{c2,0})$, $\tau \in [\tau_{c1,0}, +\infty)$ and stable for $\tau \in (\tau_{c2,0}, \tau_{c1,0})$. Hence, the number of stability switches is 2. Figs. 9 and 10 verify this conclusion. From this analysis it appears that the presence of small time delay can be beneficial, in the sense of postponing the occurrence of flutter instability. Purposefully introduced time delay may be used to improve both systems' stability and performance. Of course, time delay in control system is usually regarded as detrimental, in the sense of the system reliability.

Case 6. $g_v = 2.3\,\mathrm{N\,m\,s/rad},\ V = 25.0\,\mathrm{m/s}$

This parameter combination (g_v, V) falls into the sub-region VIII in Fig. 7, and the polynomial $F(\omega)$ has two distinct positive real roots $\omega_1 = 46.3558$ and $\omega_2 = 8.8656$ satisfying $F'(\omega_1)>0$ and $F'(\omega_2)<0$, respectively. The corresponding critical values of time delay are

$$\begin{cases} \tau_{c1,0} = 0.0983, & \tau_{c1,1} = 0.2338, & \tau_{c1,2} = 0.3694, & \tau_{c1,3} = 0.5049, & \tau_{c1,4} = 0.6405, & \tau_{c1,5} = 0.7760, \\ \tau_{c1,6} = 0.9116, & \tau_{c1,7} = 1.0471, & & & & \\ \tau_{c2,0} = 0.1650, & \tau_{c2,1} = 0.8737, & \tau_{c2,2} = 1.5824, & \tau_{c2,3} = 2.2911, & \tau_{c2,4} = 2.9998, & \tau_{c2,5} = 3.7086, \\ \tau_{c2,6} = 4.4173, & \tau_{c2,7} = 5.1260, & & & & \end{cases} \tag{35}$$

which are ranked as

$$\tau_{c1,0} < \tau_{c2,0} < \underline{\tau_{c1,1} < \tau_{c1,2} < \tau_{c1,3} < \tau_{c1,4} < \tau_{c1,5}} < \tau_{c2,1} < \tau_{c1,6} < \cdots. \tag{36}$$

It is demonstrated that the system is unstable for $\tau \in [0, +\infty)$.

Case 7. $g_v = 3.0\,\mathrm{N\,m\,s/rad},\ V = 30.0\,\mathrm{m/s}$

This parameter combination (g_v, V) falls into the sub-region IX in Fig. 7; the polynomial $F(\omega)$ has two distinct positive real roots $\omega_1 = 56.2742$ and $\omega_2 = 9.2920$ satisfying $F'(\omega_1)>0$ and $F'(\omega_2)<0$, respectively. The corresponding

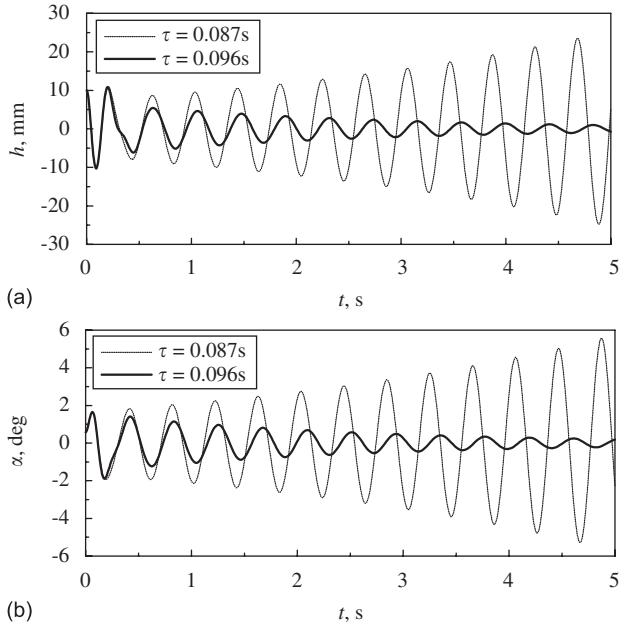

Fig. 9. Responses of the controlled aeroelastic system with time delay: (a) plunging response and (b) pitching response.

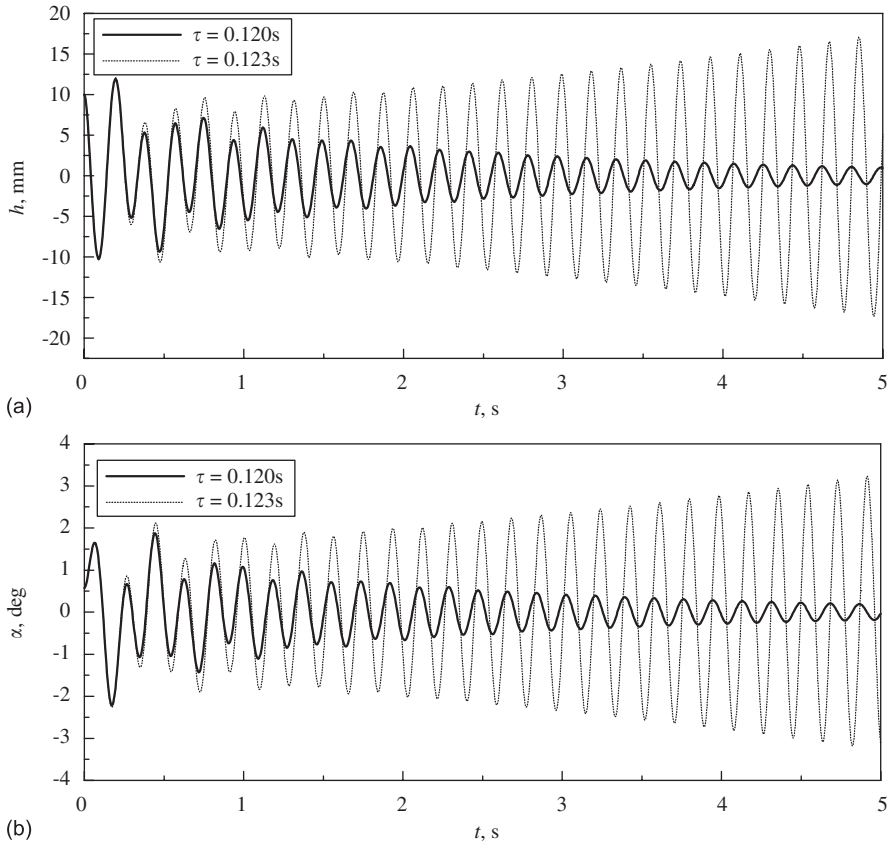

Fig. 10. Responses of the controlled aeroelastic system with time delay: (a) plunging response and (b) pitching response.

critical values of time delay are

$$\begin{cases} \tau_{c1,0}=0.0823, & \tau_{c1,1}=0.1940, & \tau_{c1,2}=0.3056, & \tau_{c1,3}=0.4173, & \tau_{c1,4}=0.5289, & \tau_{c1,5}=0.6406, \\ \tau_{c1,6}=0.7522, & \tau_{c1,7}=0.8639, & & & & \\ \tau_{c2,0}=0.1621, & \tau_{c2,1}=0.8383, & \tau_{c2,2}=1.5145, & \tau_{c2,3}=2.1907, & \tau_{c2,4}=2.8669, & \tau_{c2,5}=3.5431, \\ \tau_{c2,6}=4.2193, & \tau_{c2,7}=4.8955, & & & & \end{cases} \tag{37}$$

sorted as

$$\tau_{c1,0}<\tau_{c2,0}<\underline{\tau_{c1,1}<\tau_{c1,2}<\tau_{c1,3}<\tau_{c1,4}<\tau_{c1,5}<\tau_{c1,6}}<\tau_{c2,1}<\tau_{c1,7}<\cdots. \tag{38}$$

This reveals that the system is unstable for $\tau\in[0,+\infty)$.

Case 8. $g_v=3.0\,\mathrm{N\,m\,s/rad},\ V=24.0\,\mathrm{m/s}$

This parameter combination (g_v, V) falls into the sub-region X in Fig. 7; the polynomial $F(\omega)$ has two distinct positive real roots $\omega_1=58.2388$ and $\omega_2=6.7238$ satisfying $F'(\omega_1)>0$ and $F'(\omega_2)<0$, respectively. The corresponding critical values of time delay are

$$\begin{cases} \tau_{c1,0}=0.0806, & \tau_{c1,1}=0.1885, & \tau_{c1,2}=0.2964, & \tau_{c1,3}=0.4043, & \tau_{c1,4}=0.5122, & \tau_{c1,5}=0.6201, \\ \tau_{c1,6}=0.7280, & \tau_{c1,7}=0.8358, & & & & \\ \tau_{c2,0}=0.2206, & \tau_{c2,1}=1.1551, & \tau_{c2,2}=2.0895, & \tau_{c2,3}=3.0240, \tau_{c2,4}=3.9585, & & \tau_{c2,5}=4.8930, \\ \tau_{c2,6}=5.8274, & \tau_{c2,7}=6.7619. & & & & \end{cases} \tag{39}$$

We sort these critical time delays as follows

$$\underline{\tau_{c1,0}<\tau_{c1,1}}<\tau_{c2,0}<\tau_{c1,2}<\tau_{c1,3}<\tau_{c1,4}\quad<\tau_{c1,5}<\tau_{c1,6}<\tau_{c1,7}<\cdots. \tag{40}$$

Again, the system is unstable for $\tau\in[0,+\infty)$.

In summary, on the one hand, time delays in the control system are potential sources for causing the system to be unstable. On the other hand, we can stabilize an unstable system without any time delay by introducing an appropriate choice of time delays.

3.3. Flutter speed of the controlled system with a single time delay

In Section 3.2, the stability of the controlled system with fixed flow speed and feedback gain is studied through stability switches, and the critical time delays of the system are computed. This section focuses on the stability of the controlled system with nonzero time delay on the basis of the delay-free system.

Velocity feedback gain g_v, flutter speed V_F, and flutter frequency ω_F of the controlled system satisfies

$$D(\boldsymbol{u},\tau)=D(V,\mathrm{i}\omega,\tau)=P(V,\mathrm{i}\omega)+Q(V,\mathrm{i}\omega,g_v)\,\mathrm{e}^{-\mathrm{i}\omega\tau}=0, \tag{41}$$

where $\boldsymbol{u}=\begin{bmatrix} V_F & \omega_F \end{bmatrix}^{\mathrm{T}}$. Separating $D(V,\mathrm{i}\omega)$ into its real and imaginary parts, one obtains

$$\boldsymbol{F}(\boldsymbol{u}(\tau),\tau)=\begin{bmatrix} Q_R(\omega,g_v)\cos\omega\tau+Q_I(\omega,g_v)\sin\omega\tau+P_R(V,\omega) \\ Q_I(\omega,g_v)\cos\omega\tau-Q_R(\omega,g_v)\sin\omega\tau+P_I(V,\omega) \end{bmatrix}=0. \tag{42}$$

A standard predictor-corrector method can be used for the continuation of the above nonlinear equation. Let $\boldsymbol{u}_0=[\,V_{F0}\quad\omega_{F0}\,]^{\mathrm{T}}$ is a point on the curve $\boldsymbol{u}(\tau)$ at $\tau=\tau_0$ and assume $\boldsymbol{F}_{\boldsymbol{u}}(\boldsymbol{u}_0,\tau_0)$ is nonsingular at $(\boldsymbol{u}_0,\tau_0)$. Differentiating Eq. (42) with respect to τ at $\tau=\tau_0$ yields

$$\boldsymbol{F}_{\boldsymbol{u}}(\boldsymbol{u}_0,\tau_0)\boldsymbol{u}'(\tau_0)+\boldsymbol{F}_{\tau}(\boldsymbol{u}_0,\tau_0)=0, \tag{43}$$

where $\boldsymbol{u}'(\tau_0)$ denotes the slope of the tangent line to the solution curve at $(\boldsymbol{u}_0,\tau_0)$. Because $\boldsymbol{F}_{\boldsymbol{u}}(\boldsymbol{u}_0,\tau_0)$ is nonsingular, the set of linear algebra equations has a unique solution, thus the tangent line to the solution curve at point $(\boldsymbol{u}_0,\tau_0)$ can be written as

$$\boldsymbol{T}_0(\tau)=\boldsymbol{u}_0+(\tau-\tau_0)\boldsymbol{u}'(\tau_0). \tag{44}$$

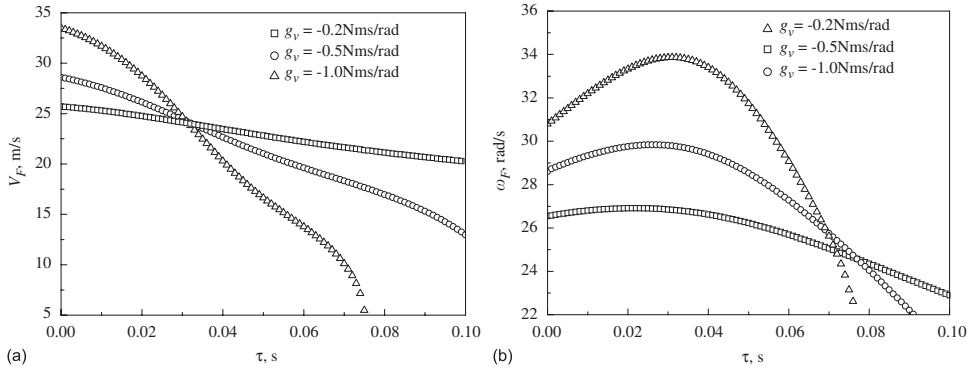

Fig. 11. Flutter speed and flutter frequency versus time delay: (a) flutter speed versus time delay and (b) flutter frequency versus time delay.

One can take the point $\boldsymbol{T}_0(\tau_1)$, τ_1 on this tangent line as an initial approximation to the solution $(\boldsymbol{u}_1, \tau_1)$, then the Newton–Raphson iteration method can be used to obtain the new solution point $(\boldsymbol{u}_1, \tau_1)$. Once the solution $\boldsymbol{u}(\tau)$ is obtained, flutter speed and frequency of the controlled system can be computed as a function of time delay τ.

As shown in Fig. 11, the flutter speed of the system decreases with the increase of time delay. It can be seen that, for the large velocity feedback gain $|g_v|$, time delay has a strong effect on flutter speed and flutter frequency of the controlled system. When $\tau = 0.032$ s, the flutter speed of the controlled system is almost not influenced by feedback gain $|g_v|$. Obviously, the continuation method provides an efficient way to compute the stability boundary of the controlled system with time delay. The above method can be easily extended to handle the system with multiple time delays.

4. Critical time delays of the controlled system with multiple time delays

In previous sections, stability of the single time-delayed system in parameter space is analyzed by using the generalized Sturm criterion for polynomials. However, systems with multiple time delays may be encountered in control engineering. In the field of aeroservoelasticity, multiple time delays may stem from the control system which includes the multiple control surfaces driven by actuators. For a system with multiple time delays, the generalized Sturm criterion is too cumbersome to be used to predict the stability of the system. Therefore, an alternative method should be developed. In practical applications, we are only interested in the critical time delays of the above system, which can be obtained by solving a quadratic eigenvalue problem.

This section handles the aeroelastic system with multiple time delays in feedback loops, given by

$$\begin{cases} \dot{\boldsymbol{X}} = \sum_{k=0}^{m} \boldsymbol{A}_k \boldsymbol{X}(t-\tau_k), & t>0, \\ \boldsymbol{X}(t) = \boldsymbol{\varphi}(t), & t \in [-\tau_m, 0], \end{cases} \tag{45}$$

where $0 = \tau_0 < \tau_1 < \cdots < \tau_m$, $\boldsymbol{A}_k \in \mathbb{R}^{n\times n}$.

We have the characteristic equation of the system in Eq. (45) as follows

$$\boldsymbol{T}(\lambda)\bar{\boldsymbol{X}} = \left(-\lambda \boldsymbol{I} + \sum_{k=0}^{m} \boldsymbol{A}_k \, \mathrm{e}^{-\tau_k \lambda}\right)\bar{\boldsymbol{X}} = 0, \quad ||\bar{\boldsymbol{X}}|| = 1. \tag{46}$$

Define operator $\boldsymbol{\Theta}$ as follows:

$$\Theta(\boldsymbol{Y}, \lambda) = \boldsymbol{T}(\lambda)\boldsymbol{Y} + \boldsymbol{Y}\boldsymbol{T}^*(\lambda) = \sum_{k=0}^{m} (\boldsymbol{A}_k \boldsymbol{Y} \, \mathrm{e}^{-\tau_k \lambda} + \boldsymbol{Y}\boldsymbol{A}_k^{\mathrm{T}} \, \mathrm{e}^{-\tau_k \bar{\lambda}}) - 2\boldsymbol{Y}\,\mathrm{Re}\lambda; \tag{47}$$

herein the asterisk denotes complex conjugate transpose, and $\bar{\lambda}$ is complex conjugate of λ.

It is easy to prove that for the given $\lambda \in \mathbb{C}$ and $\bar{\boldsymbol{X}}^*\bar{\boldsymbol{X}} = 1$, Eq. (46) is equivalent to the following expressions:

$$\Theta(\bar{\boldsymbol{X}}\bar{\boldsymbol{X}}^*, \lambda) = 0 \wedge \bar{\boldsymbol{X}}^* \boldsymbol{T}(\lambda)\bar{\boldsymbol{X}} = 0, \tag{48}$$

where the sign $\wedge$ means logical "and".

The imaginary characteristic roots play a critical role in stability analysis of the system, so substituting $\lambda = \mathrm{i}\omega$ into $\Theta(\bar{\boldsymbol{X}}\bar{\boldsymbol{X}}^*, \lambda) = 0$ in Eq. (48) and multiply with $\mathrm{e}^{\mathrm{i}\tau_{cm}\omega}$, we have

$$z^2\bar{\boldsymbol{X}}\bar{\boldsymbol{X}}^*\boldsymbol{A}_m^{\mathrm{T}} + z\sum_{k=0}^{m-1}(\boldsymbol{A}_k\bar{\boldsymbol{X}}\bar{\boldsymbol{X}}^*\,\mathrm{e}^{-\mathrm{i}\phi_k} + \bar{\boldsymbol{X}}\bar{\boldsymbol{X}}^*\boldsymbol{A}_k^{\mathrm{T}}\,\mathrm{e}^{\mathrm{i}\phi_k}) + \boldsymbol{A}_m\bar{\boldsymbol{X}}\bar{\boldsymbol{X}}^* = 0, \tag{49}$$

where

$$\begin{cases} z = \mathrm{e}^{i\tau_{cm}\omega}, \\ \tau_{cm} = \dfrac{\mathrm{Arg}(z) + 2q_m\pi}{\omega}, \quad \tau_{ck} = \dfrac{\phi_k + 2q_k\pi}{\omega}, \\ \phi_k \in [-\pi, \pi], \quad k = 1, \ldots, m-1, \\ q_s \in \mathbb{Z}, \quad s = 1, \ldots, m. \end{cases} \tag{50}$$

Substituting $\lambda = \mathrm{i}\omega$ into $\bar{\boldsymbol{X}}^*\boldsymbol{T}(\lambda)\bar{\boldsymbol{X}} = 0$ in Eq. (48), we obtain

$$\omega = -\mathrm{i}\bar{\boldsymbol{X}}^*\left(\boldsymbol{A}_m z^{-1} + \sum_{k=0}^{m-1}\boldsymbol{A}_k\,\mathrm{e}^{-i\phi_k}\right)\bar{\boldsymbol{X}}. \tag{51}$$

Note that Eq. (49) is difficult to solve directly. However, we can obtain a vectorized version of Eq. (49) through the operator vec. In matrix algebra, the vec operator can vectorize a matrix by stacking its columns (it is conventional that column rather than row stacking is used). There is an important relationship between the vec operator and the Kronecker product, that is

$$\mathrm{vec}(\boldsymbol{X}_1\boldsymbol{B}\boldsymbol{X}_2) = (\boldsymbol{X}_2^{\mathrm{T}} \otimes \boldsymbol{X}_1)\mathrm{vec}\,\boldsymbol{B}. \tag{52}$$

Once the vec operator is applied in Eq. (49), we can obtain the following quadratic eigenproblem:

$$\left(z^2\boldsymbol{A}_m \otimes \boldsymbol{I} + z\sum_{k=0}^{m-1}\boldsymbol{L}_k(\phi_k) + \boldsymbol{I} \otimes \boldsymbol{A}_m\right)\bar{\boldsymbol{Y}} = 0, \tag{53}$$

where

$$\bar{\boldsymbol{Y}} = \mathrm{vec}(\bar{\boldsymbol{X}}\bar{\boldsymbol{X}}^*), \quad \boldsymbol{L}_k(\phi_k) = \boldsymbol{I} \otimes \boldsymbol{A}_k\,\mathrm{e}^{-\mathrm{i}\phi_k} + \boldsymbol{A}_k \otimes \boldsymbol{I}\,\mathrm{e}^{\mathrm{i}\phi_k}. \tag{54}$$

Note that the above quadratic eigenproblem can be recast into the following generalized eigenvalue problem:

$$\begin{pmatrix} 0 & \boldsymbol{I} \\ \boldsymbol{I} \otimes \boldsymbol{A}_m & \sum_{k=0}^{m-1}\boldsymbol{L}_k(\phi_k) \end{pmatrix}\begin{pmatrix} \bar{\boldsymbol{Y}} \\ z\bar{\boldsymbol{Y}} \end{pmatrix} = z\begin{pmatrix} \boldsymbol{I} & 0 \\ 0 & -\boldsymbol{A}_m \otimes \boldsymbol{I} \end{pmatrix}\begin{pmatrix} \bar{\boldsymbol{Y}} \\ z\bar{\boldsymbol{Y}} \end{pmatrix}. \tag{55}$$

Eq. (50) reveals that only the unit eigenvalue will be of interest, so the Cayley transformation

$$z = \frac{1 + \mathrm{i}\sigma}{1 - \mathrm{i}\sigma} \tag{56}$$

can be applied to Eq. (55). Thus, Eq. (55) becomes

$$(\bar{\boldsymbol{A}} - \bar{\boldsymbol{B}})\bar{\boldsymbol{V}} = \sigma(\mathrm{i}\bar{\boldsymbol{A}} + \mathrm{i}\bar{\boldsymbol{B}})\bar{\boldsymbol{V}}, \tag{57}$$

where

$$\bar{\boldsymbol{A}} = \begin{pmatrix} \boldsymbol{0} & \boldsymbol{I} \\ \boldsymbol{I} \otimes \boldsymbol{A}_m & \sum_{k=0}^{m-1}\boldsymbol{L}_k(\phi_k) \end{pmatrix}, \quad \bar{\boldsymbol{B}} = \begin{pmatrix} \boldsymbol{I} & \boldsymbol{0} \\ \boldsymbol{0} & -\boldsymbol{A}_m \otimes \boldsymbol{I} \end{pmatrix}.$$

Once the real eigenvalues are found for the generalized eigenvalue problem, Eq. (57), the unit eigenvalue z can be easily obtained by Eq. (56).

We now use the theory described in this section to predict the stability of the 2-dof system with a single or multiple time delays.

Firstly, the critical time delay of the single time delay system Eq. (7) is obtained by using the quadratic eigenvalue method. Parameters used for simulation are shown in Table 1. Fig. 12 presents the critical time delays of this controlled system in parameter space (g_v, V).

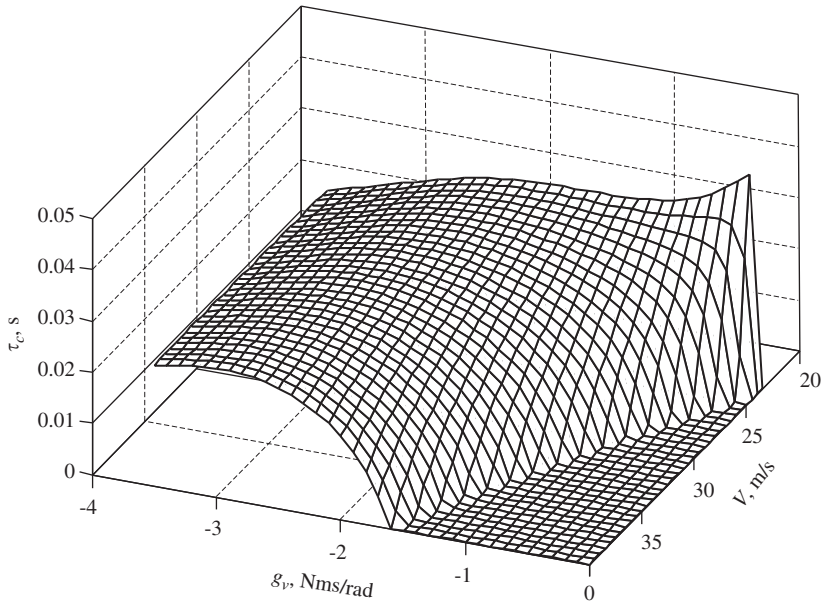

Fig. 12. Critical time delay of the controlled aeroelastic system.

Secondly, we test the present method by a controlled aeroelastic system with two time delays. Here we assume that the time delays are incommensurate. If time delays in pitching displacement and pitching velocity feedback signals are considered, the controlled aeroelastic system can be written as

$$\dot{\boldsymbol{X}} = \boldsymbol{A}_0(V)\boldsymbol{X} + \boldsymbol{A}_1(g_p)\boldsymbol{X}(t-\tau_1) + \boldsymbol{A}_2(g_v)\boldsymbol{X}(t-\tau_2), \tag{58}$$

where

$$\boldsymbol{A}_1 = \begin{bmatrix} 0 & 0 & 0 & 0 \\ 0 & 0 & 0 & 0 \\ 0 & g_p b_{32} & 0 & 0 \\ 0 & g_p b_{42} & 0 & 0 \end{bmatrix}, \quad b_{32} = c_{34}, \quad b_{42} = c_{44},$$

τ_1 and τ_2 are time delays in pitching displacement and pitching velocity, respectively. g_p and g_v are feedback gains in pitching displacement and pitching velocity, respectively.

When $\tau_1 = \tau_2 = 0$, the characteristic equation of the system Eq. (58) is given by

$$D(\lambda) = \lambda^4 + \bar{p}_3\lambda^3 + \bar{p}_2\lambda^2 + \bar{p}_1\lambda + \bar{p}_0 = 0, \tag{59}$$

where

$$\begin{aligned} \bar{p}_3 &= -a_{44} - a_{33} - g_v c_{44}, \\ \bar{p}_2 &= -a_{42} - a_{31} + a_{33}a_{44} - a_{43}a_{34} + g_v(a_{33}c_{44} - a_{43}c_{34}) - g_p b_{42}, \\ \bar{p}_1 &= -a_{43}a_{32} + a_{42}a_{33} + a_{31}a_{44} - a_{41}a_{34} + g_v(a_{31}c_{44} - a_{41}c_{34}) + g_p(a_{33}b_{42} - a_{43}b_{32}), \\ \bar{p}_0 &= a_{31}a_{42} - a_{41}a_{32} + g_p(a_{31}b_{42} - a_{41}b_{32}). \end{aligned}$$

The corresponding Routh–Hurwitz condition is

$$\begin{cases} Q_1 = \bar{p}_3 > 0, \\ Q_2 = \bar{p}_2 > 0, \\ Q_3 = \bar{p}_0 > 0, \\ Q_4 = \bar{p}_1(\bar{p}_3\bar{p}_2 - \bar{p}_1) - \bar{p}_3^2\bar{p}_0 > 0. \end{cases} \tag{60}$$

As the first insight to the system, the flutter speed of the controlled system free of time delay is computed, as shown in Fig. 13. To compute the critical time delays of the system, we take g_p as $-120\,\mathrm{N\,m/rad}$ and g_v as $-0.8\,\mathrm{N\,m/rad}$. In this case we know that the flutter speed V_F of the delay-free system is 35.7 m/s. Here the flow speed V is taken as 30 m/s in simulation, which is lower than the flutter speed 35.7 m/s. The critical time delay curves on the plane of (τ_1, τ_2) are shown in Fig. 14. Obviously, the system will undergo stability switches as these two time delays vary from zero to infinity. Usually, only the smallest critical time delay will be of interest.

Fig. 15 shows the enlarged curve in the rectangular region of Fig. 14. In Fig. 15, points a–g are critical time delays for $\tau_1 = 0$, these critical time delays are given in Table 4. It is easy to examine that the system is stable when τ_1 and τ_2 fall into the shadow regions in Fig. 15(a). As shown in Fig. 15(b), on the plane of (τ_1, τ_2), we select a point with $\tau_1 = 0.001$ s and $\tau_2 = 0.018$ s in the stable region, and another point with $\tau_1 = 0.001$ s and $\tau_2 = 0.019$ s in the outer of the stable region. The responses of the system for these two sets of time delays are shown in Fig. 16. This proves that the quadratic eigenvalue method gives the correct stable regions.

As shown in Fig. 17, with the increase of flow speed, the stable regions of the system become small. In particular, when flow speed ($V = 36$ m/s is used for simulation) is larger than flutter speed of the controlled system free of time delays, there still exists the stable region, as shown in Fig. 17(c). To verify this phenomenon, time delays $\tau_1 = 0.001$ s, $\tau_2 = 0.01$ s (see the point in Fig. 17(c)), and $V = 36$ m/s are used for simulation. It is clear from Fig. 18 that the motion damps out. Therefore, we conclude that one can stabilize an aeroelastic system by introducing an appropriate choice of small time delays.

5. The rightmost eigenvalues of the controlled system with multiple time delays

The principal difficulty in studying delay differential equations (DDEs) lies in its special transcendental character. Delay equations always lead to an infinite number of characteristic roots. However, only a finite number have real parts greater than a given constant. Therefore, stability of the time-delayed system can be determined by computing the rightmost eigenvalues of the DDEs. Numerical approaches for characteristic roots computation of linear autonomous DDEs have been recently proposed (Breda et al., 2005; Breda, 2006). They are based on the discretization of either the solution operator or the infinitesimal generator of the original equation. In this section, the rightmost roots of the controlled aeroelastic system with time delays are computed through the infinitesimal generator approximation.

For the aeroelastic system (45) with multiple time delays, the stability of the system can be determined by eigenvalues of the following characteristic equation:

$$\det(\boldsymbol{T}(\lambda)) = \det\left(-\lambda \boldsymbol{I} + \sum_{k=0}^{m} \boldsymbol{A}_k \, \mathrm{e}^{-\tau_k \lambda}\right) = 0. \tag{61}$$

For the purpose of stability analysis, a numerical method that automatically computes the rightmost roots of Eq. (61) would be of interest. Note that the solution operator $\boldsymbol{S}(t)$, $t \geqslant 0$ of Eq. (45) is defined by the relation

$$\boldsymbol{S}(t)\boldsymbol{\varphi}(\theta) = \boldsymbol{X}_t(\theta), \quad \boldsymbol{\varphi} \in \boldsymbol{D}_s, \tag{62}$$

where $\boldsymbol{D}_s = \boldsymbol{C}_B([-\tau_m, 0], \mathbb{R}^n)$, $\boldsymbol{C}_B$ is Banach space, and $\boldsymbol{X}_t(\theta) = \boldsymbol{X}(t+\theta)$, $\theta \in [-\tau_m, 0]$. The infinitesimal generator $\boldsymbol{A}$ of $\boldsymbol{S}(t)$ is defined as

$$\begin{cases} \boldsymbol{A}\boldsymbol{\varphi}(\theta) = \dot{\boldsymbol{\varphi}}(\theta), \quad \boldsymbol{\varphi} \in \boldsymbol{D}_g(\boldsymbol{A}), \\ \boldsymbol{D}_g(\boldsymbol{A}) = \left\{ \boldsymbol{\phi} \in \boldsymbol{D}_s | \dot{\boldsymbol{\varphi}} \in \boldsymbol{D}_s \text{ and } \dot{\boldsymbol{\varphi}}(0) = \sum_{k=0}^{m} \boldsymbol{A}_k \boldsymbol{\varphi}(-\tau_k) \right\}. \end{cases} \tag{63}$$

So, Eq. (45) can be recast as an abstract Cauchy problem of the form

$$\begin{cases} \dfrac{\mathrm{d}\boldsymbol{X}_t}{\mathrm{d}t} = \boldsymbol{A}\boldsymbol{X}_t, \quad t \geqslant 0, \\ \boldsymbol{X}_0 = \boldsymbol{\varphi}. \end{cases} \tag{64}$$

From the above equations, one can obtain the following result:

$$\det(\boldsymbol{T}(\lambda)) = 0 \Leftrightarrow \lambda \in \sigma(\boldsymbol{A}), \tag{65}$$

where $\sigma(\cdot)$ is the spectrum operator. Since the spectrum of the solution generator consists of the characteristic roots, such roots can be computed as the eigenvalues of suitable matrices approximating this infinitesimal generator.

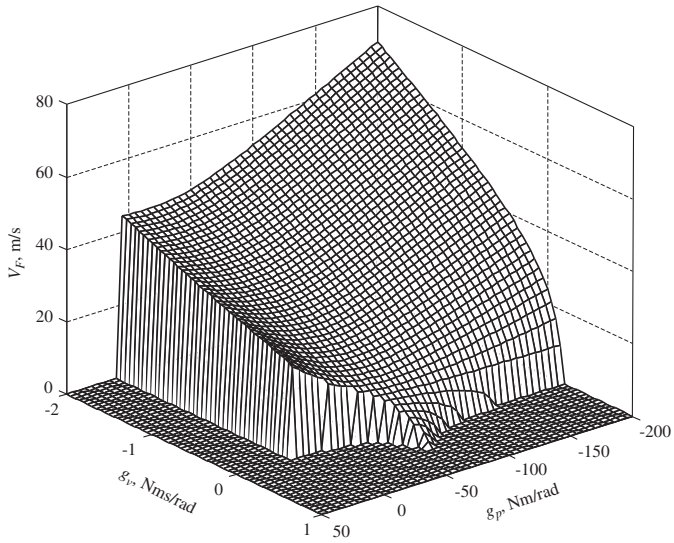

Fig. 13. Flutter speed versus feedback gain, $\tau_1 = \tau_2 = 0$.

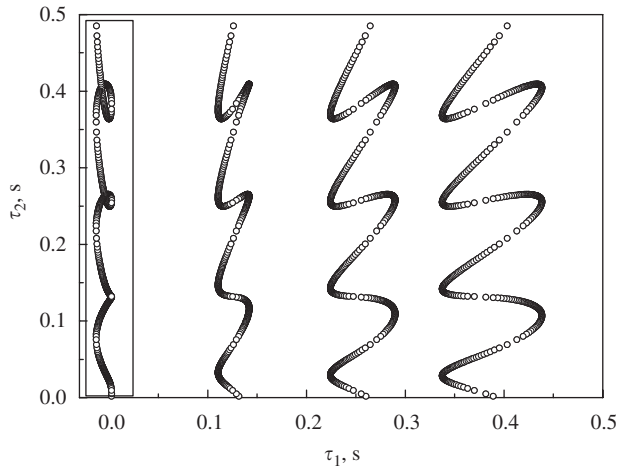

Fig. 14. Critical time delay curves for controlled aeroelastic system with two time delays: $V = 30\,\mathrm{m/s}$, $g_p = -120\,\mathrm{N\,m/rad}$, $g_v = -0.8\,\mathrm{N\,m\,s/rad}$.

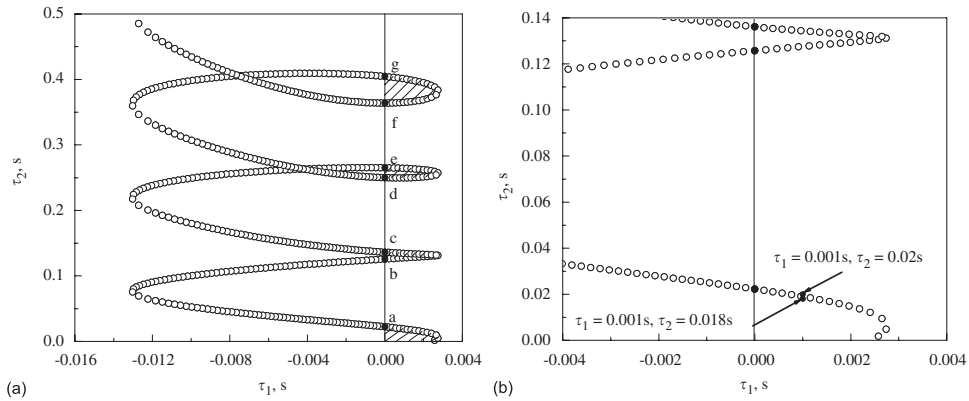

Fig. 15. Enlarged curve in the rectangle region of Fig. 14.

Table 4
Critical time delays of the system for $\tau_1 = 0$

Point a	Point b	Point c	Point d	Point e	Point f	Point g
$\tau_2 = 0.0222$ s	$\tau_2 = 0.1257$ s	$\tau_2 = 0.1361$ s	$\tau_2 = 0.2499$ s	$\tau_2 = 0.2651$ s	$\tau_2 = 0.3638$ s	$\tau_2 = 0.4044$ s

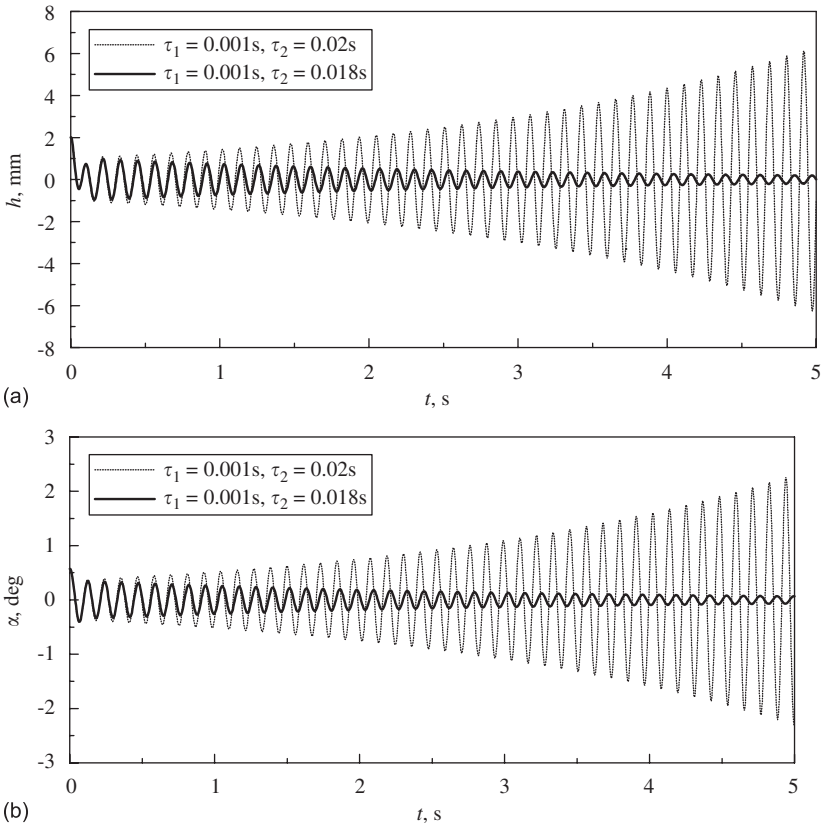

Fig. 16. Validation of the stability for the controlled aeroelastic system with two time delays for $V = 30$ m/s, $g_p = -120$ N m/rad, $g_v = -0.8$ N m s/rad: (a) plunge response and (b) pitching response.

To make a matrix approximation to the infinitesimal generator $\boldsymbol{A}$, let us consider the following Chebyshev division points in $[-\tau_m, 0]$:

$$\theta_{N,i} = \frac{\tau_m}{2}\left(\cos\left(\mathrm{i}\frac{\pi}{N}\right) - 1\right), \quad i = 0, 1, \ldots, N, \tag{66}$$

where $-\tau_m = \theta_{N,N} < \theta_{N,N-1} < \cdots < \theta_{N,1} < \theta_{N,0} = 0$. Let $\boldsymbol{\varphi}_N$ be an approximation of $\boldsymbol{\varphi}$, and can be written as

$$\boldsymbol{\varphi}_N(\theta) = \sum_{j=0}^{N} [l_j(\theta) \otimes \boldsymbol{I}_n]\boldsymbol{f}_j, \tag{67}$$

where $\otimes$ denotes Kronecker products, $l_j(\cdot)$ is the Lagrange interpolating polynomial, and $\boldsymbol{f}_j = \boldsymbol{\varphi}(\theta_{N,j})$.

On the basis of splicing condition and Eq. (63), one obtains

$$\begin{cases} (\boldsymbol{A}\boldsymbol{\varphi})(0) = \dot{\boldsymbol{\varphi}}(0) \simeq \sum\limits_{k=0}^{m} \boldsymbol{A}_k \boldsymbol{\varphi}_N(-\tau_k) = (\boldsymbol{A}_N \boldsymbol{f})_0, \\ (\boldsymbol{A}\boldsymbol{\varphi})(\theta_{N,i}) = \dot{\boldsymbol{\varphi}}(\theta_{N,i}) \simeq \dot{\boldsymbol{\varphi}}_N(\theta_{N,i}) = (\boldsymbol{A}_N \boldsymbol{f})_i, \quad i = 1, 2, \ldots, N, \end{cases} \tag{68}$$

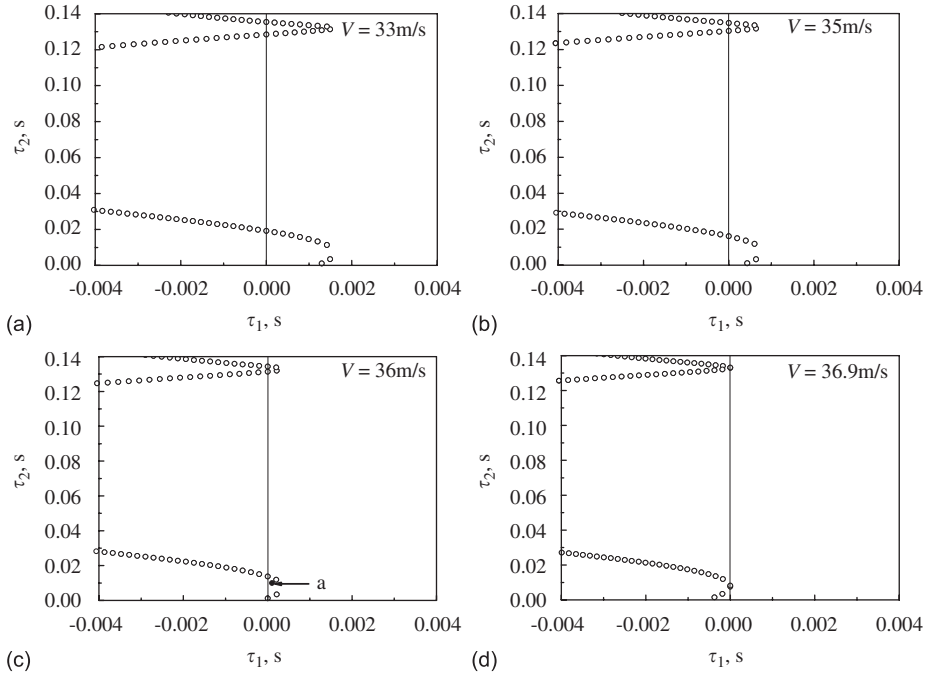

Fig. 17. Stable region of the controlled aeroelastic system with two time delays for $g_p = -120\,\mathrm{N\,m/rad}$, $g_v = -0.8\,\mathrm{N\,m\,s/rad}$.

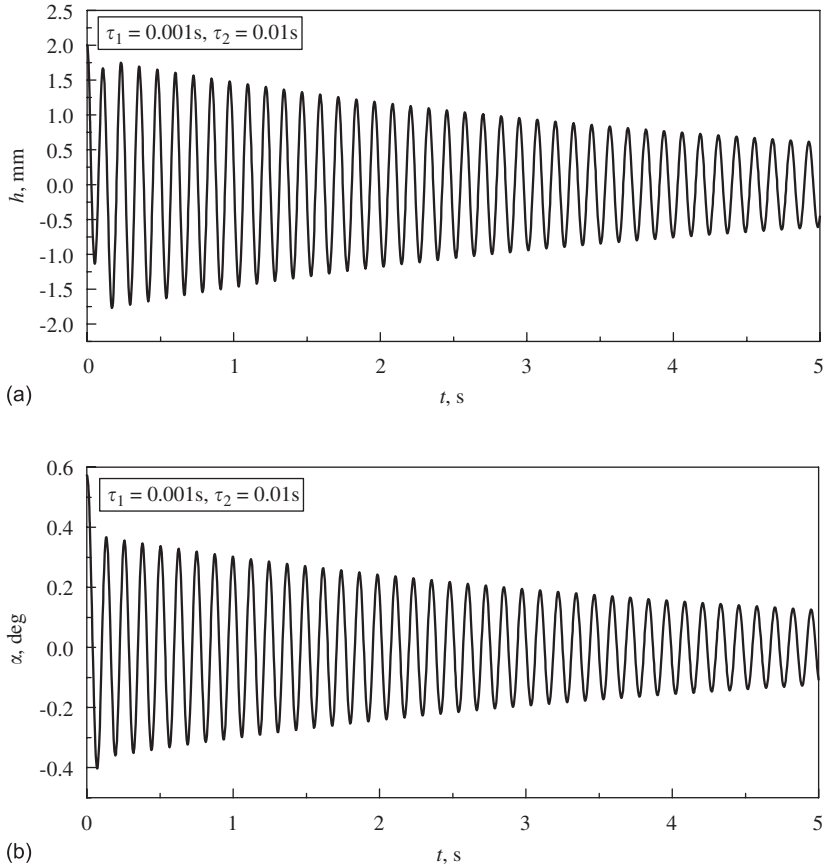

Fig. 18. Responses of the controlled aeroelastic system for $V = 36\,\mathrm{m/s}$, $g_p = -120\,\mathrm{N\,m/rad}$, $g_v = -0.8\,\mathrm{N\,m\,s/rad}$: (a) plunging response and (b) pitching response.

where $\boldsymbol{A}_N$ denotes the discrete form of $\boldsymbol{A}$, and $\boldsymbol{f}=[\boldsymbol{f}_0^{\mathrm{T}},\boldsymbol{f}_1^{\mathrm{T}},\ldots,\boldsymbol{f}_N^{\mathrm{T}}]^{\mathrm{T}}$. Obviously, Eq. (69) can be recast as

$$\boldsymbol{A}_N\begin{Bmatrix}\boldsymbol{f}_0\\ \boldsymbol{f}_1\\ \vdots\\ \boldsymbol{f}_N\end{Bmatrix}=\begin{bmatrix}\boldsymbol{e}_0 & \boldsymbol{e}_1 & \cdots & \boldsymbol{e}_N\\ \boldsymbol{g}_{10} & \boldsymbol{g}_{11} & \cdots & \boldsymbol{g}_{1N}\\ \vdots & \vdots & \ddots & \vdots\\ \boldsymbol{g}_{N0} & \boldsymbol{g}_{N1} & \cdots & \boldsymbol{g}_{NN}\end{bmatrix}\begin{Bmatrix}\boldsymbol{f}_0\\ \boldsymbol{f}_1\\ \vdots\\ \boldsymbol{f}_N\end{Bmatrix}=\begin{Bmatrix}\sum_{k=0}^{m}\boldsymbol{A}_k\boldsymbol{\varphi}_N(-\tau_k)\\ \dot{\boldsymbol{\varphi}}_N(\theta_{N,1})\\ \vdots\\ \dot{\boldsymbol{\varphi}}_N(\theta_{N,N})\end{Bmatrix}. \tag{69}$$

The elements in matrix $\boldsymbol{A}_N$ can be obtained as

$$\boldsymbol{e}_j=\sum_{k=0}^{m}\boldsymbol{A}_k[l_j(-\tau_k)\otimes\boldsymbol{I}_n],\quad \boldsymbol{g}_{ij}=\dot{l}_j(\theta_{N,i})\otimes\boldsymbol{I}_n,\quad i=1,\ldots,N,\quad j=0,1,\ldots,N. \tag{70}$$

Thus, the rightmost eigenvalues of the above system can be obtained by solving the corresponding eigenvalue problem for matrix $\boldsymbol{A}_N$.

To illustrate the effectiveness of the present approach, we attempt to compute the rightmost eigenvalues of the aeroelastic system (7). Fig. 19(a) shows the first eleven rightmost roots of the system when $g_v=-1.0\,\mathrm{N\,m\,s/rad}$ and $V=25.0\,\mathrm{m/s}$. The critical time delay of the system is $\tau_c=0.0293\,\mathrm{s}$, which is the same as that obtained in Case 1 (see Section 3.2). When $g_v=-3.0\,\mathrm{N\,m\,s/rad}$ and $V=30.0\,\mathrm{m/s}$, as shown in Fig. 19(b), with an increase of time delay, an eigenvalue (non-system poles) streams in from $-\infty$ in the complex plane and becomes "the most dangerous eigenvalue" that determines the stability of the system. In this case the classical eigenvalue continuation method is unable to predict the critical time delay if one takes the eigenvalues of the delay-free system as starting points. However, the present method gives the correct result, that is $\tau_c=0.0625\,\mathrm{s}$, which is identical to that obtained in Case 3 (see Section 3.2). As shown in Fig. 19(c), if we take $g_v=1.0\,\mathrm{N\,m\,s/rad}$ and $V=25\,\mathrm{m/s}$, the controlled aeroelastic system is unstable for $\tau\in[0,0.0904\,\mathrm{s})$, stable for $\tau\in(0.0904\,\mathrm{s},0.1221\,\mathrm{s})$, and unstable again for $\tau>0.1221\,\mathrm{s}$. When $g_v=2.3\,\mathrm{N\,m\,s/rad}$ and $V=25\,\mathrm{m/s}$, the controlled aeroelastic system is unstable for $\tau\geqslant 0$, as shown in Fig. 19(d).

Next, the controlled aeroelastic system (58) with two time delays is considered to perform the further validation test for the present method. Fig. 20 shows the effect of time delays on flutter speed of the controlled aeroelastic system when

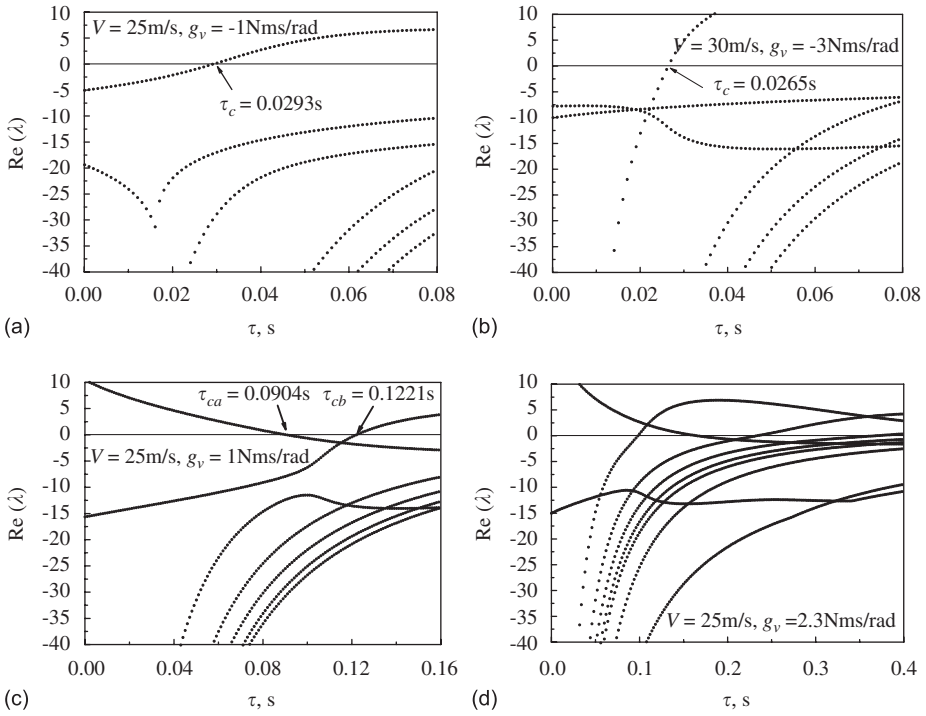

Fig. 19. Rightmost eigenvalues of the system (7) versus time delay for different flow speeds and gains.

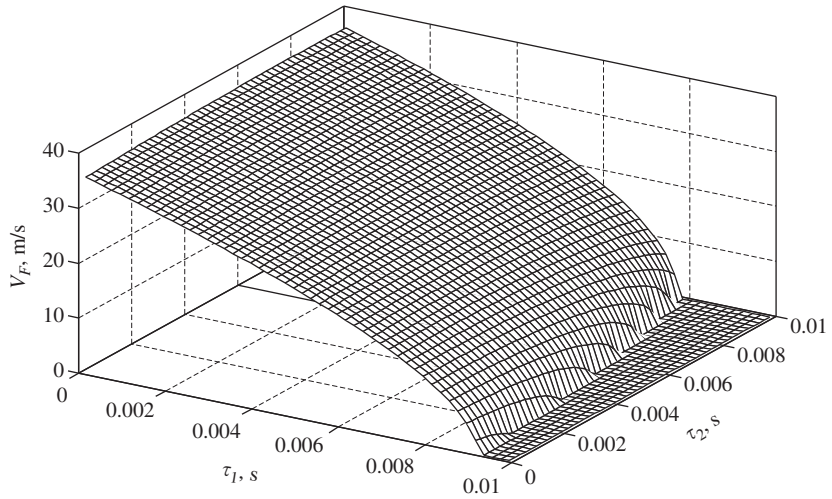

Fig. 20. Flutter speed versus time delays for $g_p = -120\,\mathrm{N\,m/rad}$, $g_v = -0.8\,\mathrm{N\,m\,s/rad}$.

$g_p = 120\,\mathrm{N\,m/rad}$ and $g_v = -0.8\,\mathrm{N\,m\,s/rad}$. It can be seen that the flutter speed of the system is strongly influenced by time delay τ_1. One can validate the result shown in Fig. 20 by computing time history responses of the system when time delays τ_1 and τ_2 are given. It is important to point out that the choice of N in the discretization scheme turns out to be crucial in saving computational time. Here, we use $N = 20$ for the above simulation.

6. Conclusions

A detailed study is conducted regarding the stability of a two-dimensional airfoil with time-delayed feedback control. The present work proves that the delay-independently stable domain of the controlled aeroelastic system occupies a small region of parameter space, and exists only for the case when the flow speed is less than the flutter speed of the system in the absence of control. If the parameters fall outside of the delay-independently stable region, the system under different parameter combinations may undergo the stability switches, that is, the initially stable system may become unstable at each boundary crossing or *vice versa*. An interesting phenomenon is that a small time delay in the feedback control can stabilize an aeroelastic system, which is initially unstable under delay-free control. Simulation results for the multiple time delays case show that the quadratic eigenvalue method and the infinitesimal generator method are very efficient and reliable for predicting the stability of the linear time-invariant system with multiple time delays.

Acknowledgement

This work was supported in part by The National Natural Science Foundation of China under Grant no. 10532050.

Appendix A

The coefficients of Eqs. (5) and (6) are given as follows:

$$c_0 = m + \pi\rho_a b^2 s_p, \quad c_1 = mx_\alpha - \pi\rho_a b^3 \bar{a} s_p, \quad c_2 = c_h + 2\pi\rho_a V b s_p,$$
$$c_3 = \pi\rho_a b^2 V s_p + 2\pi\rho_a V b^2 (0.5 - \bar{a}) s_p, \quad c_4 = k_h, \quad c_5 = 2\pi\rho_a V^2 b s_p,$$
$$d_0 = mx_\alpha - \pi\rho_a b^3 \bar{a} s_p, \quad d_1 = mr_\alpha^2 + \pi\rho_a b^4 (0.125 + \bar{a}^2) s_p, \quad d_2 = -2\pi\rho_a V b^2 (0.5 + \bar{a}) s_p,$$
$$d_3 = c_\alpha - 2\pi\rho_a b^3 V (0.5 - \bar{a}) \bar{a} s_p, \quad d_4 = 0, \quad d_5 = k_\alpha - 2\pi\rho_a V^2 b^2 (0.5 + \bar{a}) s.$$

Appendix B

The matrices $\boldsymbol{A}_0$ and $\boldsymbol{A}_2$ are given by

$$\boldsymbol{A}_0=\begin{bmatrix}0&0&1&0\\0&0&0&1\\a_{31}&a_{32}&a_{33}&a_{34}\\a_{41}&a_{42}&a_{43}&a_{44}\end{bmatrix},\quad \boldsymbol{A}_2=\begin{bmatrix}0&0&0&0\\0&0&0&0\\0&0&0&g_vc_{34}\\0&0&0&g_vc_{44}\end{bmatrix},$$

$$a_{31}=\frac{c_4d_1-c_1d_4}{d_0c_1-c_0d_1},\quad a_{32}=\frac{c_5d_1-c_1d_5}{d_0c_1-c_0d_1},\quad a_{33}=\frac{c_2d_1-c_1d_2}{d_0c_1-c_0d_1},\quad a_{34}=\frac{c_3d_1-c_1d_3}{d_0c_1-c_0d_1},$$

$$a_{41}=\frac{c_0d_4-c_4d_0}{d_0c_1-c_0d_1},\quad a_{42}=\frac{c_0d_5-c_5d_0}{d_0c_1-c_0d_1},\quad a_{43}=\frac{c_0d_2-c_2d_0}{d_0c_1-c_0d_1},\quad a_{44}=\frac{c_0d_3-c_3d_0}{d_0c_1-c_0d_1},$$

$$c_{34}=\frac{c_1}{d_0c_1-c_0d_1},\quad c_{44}=-\frac{c_0}{d_0c_1-c_0d_1}.$$

Appendix C

$$P(\lambda)=\lambda^4+p_3\lambda^3+p_2\lambda^2+p_1\lambda+p_0,\quad Q(\lambda)=q_3\lambda^3+q_2\lambda^2+q_1\lambda,$$

$$p_3=-a_{44}-a_{33},\quad p_2=-a_{42}-a_{31}+a_{33}a_{44}-a_{43}a_{34},\quad p_1=-a_{43}a_{32}+a_{42}a_{33}+a_{31}a_{44}-a_{41}a_{34},$$

$$p_0=a_{31}a_{42}-a_{41}a_{32},\quad q_3=-g_vc_{44},\quad q_2=g_v(a_{33}c_{44}-a_{43}c_{34}),\quad q_1=g_v(a_{31}c_{44}-a_{41}c_{34}),$$

$$P(\lambda)=\lambda^4+p_3\lambda^3+p_2\lambda^2+p_1\lambda+p_0,\quad Q(\lambda)=q_3\lambda^3+q_2\lambda^2+q_1\lambda,$$

$$p_3=-a_{44}-a_{33},\quad p_2=-a_{42}-a_{31}+a_{33}a_{44}-a_{43}a_{34},\quad p_1=-a_{43}a_{32}+a_{42}a_{33}+a_{31}a_{44}-a_{41}a_{34},$$

$$p_0=a_{31}a_{42}-a_{41}a_{32},\quad q_3=-g_vc_{44},\quad q_2=g_v(a_{33}c_{44}-a_{43}c_{34}),\quad q_1=g_v(a_{31}c_{44}-a_{41}c_{34}).$$

Appendix D

$$\begin{aligned}
d_0 &= -b_1,\\
d_1 &= -8b_2+3b_1^2,\\
d_2 &= b_1^2b_2+3b_1b_3-4b_2^2,\\
d_3 &= -3b_1^3b_3+b_1^2b_2^2-6b_1^2b_4+14b_1b_2b_3-4b_2^3+16b_2b_4-18b_3^2,\\
d_4 &= -b_1^2b_2^2b_3-18b_1b_2b_3^2+7b_1^2b_3b_4+12b_1b_2^2b_4-48b_2b_3b_4+4b_2^3b_3+16b_1b_4^2+27b_3^3+4b_1^3b_3^2-3b_1^3b_2b_4,\\
d_5 &= -27b_1^4b_4^2+18b_1^3b_2b_3b_4-4b_1^3b_3^3-4b_1^2b_2^3b_4+b_1^2b_2^2b_3^2+144b_1^2b_2b_4^2-6b_1^2b_3^2b_4-80b_1b_2^2b_3b_4+18b_1b_2b_3^3\\
&\quad -192b_1b_3b_4^2+16b_2^4b_4-4b_2^3b_3^2-128b_2^2b_4^2+144b_2b_3^2b_4+256b_4^3-27b_3^4,\\
d_6 &= b_4>0.
\end{aligned}$$

References

Bhoi, N., Singh, S.N., 2005. Control of unsteady aeroelastic system via state dependent Riccati equation method. Journal of Guidance, Control, and Dynamics 28, 78–84.

Breda, D., 2006. Solution operator approximations for characteristic roots of delay differential equations. Applied Numerical Mathematics 56, 305–317.

Breda, D., Maset, S., Vermiglio, R., 2005. Pseudospectral differencing methods for characteristic roots of delay differential equations. SIAM Journal on Scientific Computing 27, 482–495.

Hassard, B.D., 1997. Counting roots of the characteristic function for linear delay differential systems. Journal of Differential Equations 136, 222–235.

Hu, H.Y., Wang, Z.H., 2002. Dynamics of Controlled Mechanical Systems with Delayed Feedback. Springer, Heidelberg, pp. 1–294.

Hu, H.Y., Dowell, E.H., Virgin, L.N., 1998. Stability estimation of high dimensional vibrating system under state delay feedback control. Journal of Sound and Vibration 214, 497–511.

Ko, J., Strganac, T.W., Kurdila, A.J., 1999. Adaptive feedback linearization for the control of a typical wing section with structural nonlinearity. Nonlinear Dynamics 18, 289–301.

Kolmanovski, V.B., Nosov, V.R., 1986. Stability of Functional Differential Equations. Academic Press, London.

Librescu, L., Marzocca, P., 2002. Advances in the linear/nonlinear control of aeroelastic structural systems. Acta Mechanica 178, 147–186.

Librescu, L., Marzocca, P., 2005. Aeroelasticity of 2D lifting surfaces with time-delayed feedback control. Journal of Fluids and Structures 20, 197–215.

Marzocca, P., Librescu, L., 2005. Time-delay effects on linear/nonlinear feedback control of simple aeroelastic systems. Journal of Guidance Control and Dynamics 28, 53–62.

Niculescu, S.I., 2001. Delay Effects on Stability, A Robust Control Approach. Lecture Notes in Control and Information Sciences, col. 269. Springer, London.

Olgac, N., Sipahi, R., 2002. An exact method for the stability analysis of time-delayed linear time-invariant systems. IEEE Transactions on Automatic Control 47, 793–797.

Platanitis, G., Strganac, T.W., 2004. Control of a nonlinear wing section using leading and trailing edge surfaces. Journal of Guidance, Control, and Dynamics 27, 52–58.

Ramesh, M., Narayanan, S., 2001. Controlling chaotic motions in a two-dimensional airfoil using time-delayed feedback. Journal of Sound and Vibration 239, 1037–1049.

Stépán, G., 1989. Retarded Dynamical Systems: Stability and Characteristic Functions. Pitman Research Notes in Mathematics Series, vol. 210. Longman Scientific and Technical, Wiley, New York.

Wang, Z.H., Hu, H.Y., 2000. Stability switches of the time delayed dynamic systems with unknown parameters. Journal of Sound and Vibration 233, 215–233.

Yuan, Y., Yu, P., Librescu, L., Marzocca, P., 2004. Aeroelasticity of time-delayed feedback control of two-dimensional supersonic lifting surfaces. Journal of Guidance Control and Dynamics 27, 795–803.

Zhao, Y.H., 2007. Aeroelasticity and Control. Academic Press, Beijing (in Chinese).